nature biomedical engineering

Article

https://doi.org/10.1038/s41551-024-01208-4

Dendritic-cell-targeting virus-like particles as potent mRNA vaccine carriers

Received: 21 October 2022

Accepted: 31 March 2024

Published online: 07 May 2024

Check for updates

Di Yin[1,11], Yiye Zhong[1,11], Sikai Ling[1,2,11], Sicong Lu[1,11], Xiaoyuan Wang[2,11], Zhuofan Jiang[1], Jie Wang[1], Yao Dai[1], Xiaolong Tian[3], Qijing Huang[1], Xingbo Wang[4], Junsong Chen[1], Ziying Li[1], Yang Li[1], Zhijue Xu[1], Hewei Jiang[1], Yuqing Wu[5], Yi Shi[6], Quanjun Wang[7], Jianjiang Xu[5], Wei Hong[8,9], Heng Xue[8,9], Hang Yang[8,9,10], Yan Zhang[1], Lintai Da[1], Ze-guang Han[1], Sheng-ce Tao[1], Ruijiao Dong[1], Tianlei Ying[3], Jiaxu Hong[5] ✉ & Yujia Cai[1] ✉

Messenger RNA vaccines lack specificity for dendritic cells (DCs)—the most effective cells at antigen presentation. Here we report the design and performance of a DC-targeting virus-like particle pseudotyped with an engineered Sindbis-virus glycoprotein that recognizes a surface protein on DCs, and packaging mRNA encoding for the Spike protein of severe acute respiratory syndrome coronavirus 2 (SARS-CoV-2) or for the glycoproteins B and D of herpes simplex virus 1. Injection of the DC-targeting SARS-CoV-2 mRNA vaccine in the footpad of mice led to substantially higher and durable antigen-specific immunoglobulin-G titres and cellular immune responses than untargeted virus-like particles and lipid–nanoparticle formulations. The vaccines also protected the mice from infection with SARS-CoV-2 or with herpes simplex virus 1. Virus-like particles with preferential uptake by DCs may facilitate the development of potent prophylactic and therapeutic vaccines.

Vaccines are among the most effective medical interventions in history. They are estimated to save 2.5 million lives globally each year[1]. However, many diseases are still without effective vaccines. In fact, there are no prophylactic or therapeutic vaccines for the human immunodeficiency virus (HIV), the herpes simplex virus (HSV)-1 and HSV-2 (refs. 2–5). For some viruses, such as the hepatitis B virus and the human papilloma virus, existing vaccines are only preventive and do not eliminate an established infection[6,7]. The development of vaccines against non-infectious diseases, such as cancer, is still in the early stages, with marginal success in clinical trials assessing the treatment of melanoma and glioblastoma[8,9]. These health threats motivate the further development and improvement of vaccine technologies.

The success of the Moderna (mRNA-1273) and Pfizer/BioNTech (BNT162b2) vaccines against coronavirus disease 2019 (COVID-19) dramatically boosted the development of messenger RNA vaccines[10–13]. As mRNA is vulnerable to degradation by nucleases and cannot enter cells by itself, a variety of carriers have been developed for mRNA

[1]Key Laboratory of Systems Biomedicine (Ministry of Education), Shanghai Center for Systems Biomedicine, Shanghai Jiao Tong University, Shanghai, China. [2]BDGENE Therapeutics, Shanghai, China. [3]MOE/NHC/CAMS Key Laboratory of Medical Molecular Virology, School of Basic Medical Sciences, Fudan University, Shanghai, China. [4]MOA Key Laboratory of Animal Virology, Zhejiang University Center for Veterinary Sciences, Hangzhou, China. [5]Department of Ophthalmology and Vision Science, Shanghai Eye, Ear, Nose and Throat Hospital, Fudan University, Shanghai, China. [6]Bio-X Institutes, Key Laboratory for the Genetics of Developmental and Neuropsychiatric Disorders, Shanghai Jiao Tong University, Shanghai, China. [7]National Beijing Center for Drug Safety Evaluation and Research, State Key Laboratory of Medical Countermeasures and Toxicology, Institute of Pharmacology and Toxicology, Academy of Military Sciences, Beijing, China. [8]CAS Key Laboratory of Special Pathogens and Biosafety, Center for Biosafety Mega-Science, Wuhan Institute of Virology, Chinese Academy of Sciences, Wuhan, China. [9]University of Chinese Academy of Sciences, Beijing, China. [10]Hubei Jiangxia Laboratory, Wuhan, China. [11]These authors contributed equally: Di Yin, Yiye Zhong, Sikai Ling, Sicong Lu, Xiaoyuan Wang. ✉e-mail: jiaxu.hong@fdeent.org; yujia.cai@sjtu.edu.cn

transfer, including lipid nanoparticles (LNPs), polymers, peptides, virus-like replicon particles and dendritic cells (DCs)[14]. LNPs are now the favoured carrier; however, the currently approved LNP–mRNA vaccine is not cell-specific and can be taken up by almost any cell type near or far from the site of injection, including liver cells[15,16]. Moreover, even though mRNA vaccines against severe acute respiratory syndrome coronavirus 2 (SARS-CoV-2) are effective at preventing severe outcomes of COVID-19, they do not fully control virus transmission[17]. In addition, the potential of mRNA vaccines beyond SARS-CoV-2 infections awaits further exploration.

DCs are the major antigen-presenting cells (APCs) and are critical for vaccine function by instigating T-cell immune responses through antigen processing and presentation to T cells[18,19] and by processing antigens for presentation to B cells to induce antibody responses[20,21]. The DC-based vaccine Provenge has been approved by the US Food and Drug Administration for the treatment of prostate cancer; however, it is produced ex vivo by activating isolated APCs from patients, and its production is labour-intensive, which limits its availability to a broader population. Moreover, non-professional APCs translating antigen mRNAs may become targets of cytotoxic T lymphocytes ($CD8^+$ T-cells)-mediated killing, which has been linked to 'COVID arm', a condition that develops in some patients after receiving the mRNA-1273 SARS-CoV-2 vaccine[22,23]. Furthermore, antibody-dependent cellular cytotoxicity may destroy cells that have antigen proteins inserted into them or secreted by them and associated with their plasma membrane[22,24]. Therefore, targeting DCs in situ is the direction of the next generation of mRNA vaccines. This would simplify the manufacturing process, lower the cost and improve the safety of the vaccines. DC-specific intercellular adhesion molecule 3-grabbing non-integrin (DC-SIGN) is the pattern-recognition receptor and adhesion receptor of DCs. It plays an important role in DC migration and adhesion, the inflammatory response, T-cell activation and the initiation of the immune response[25]. Recombinant lentiviral vectors pseudotyped with Sindbis-virus glycoprotein as a ligand for DC-SIGN have shown potentially improved performance over non-specific lentiviral vectors; however, the risk of insertional mutagenesis is a limiting factor for their clinical translation[26]. Although LNPs have been conjugated to specific antibodies or ligands to acquire DC specificity, evidence for the efficacy of LNP-based DC-targeting mRNA vaccines is still rare[22].

In this Article, we report a DC-targeting virus-like particle (DVLP)-based mRNA-vaccine technology. The DVLP-delivered antigen mRNA elicited a strong and durable adaptive immune response. We found that the DVLP elicited a significantly greater antigen-specific immunoglobulin G (IgG) response and T-cell response than non-specific virus-like particles (VLPs) and LNPs. Importantly, the DVLP-based mRNA vaccine efficiently protected mice from live-virus infection in both SARS-CoV-2 and HSV-1 infection models 3 days and 6 days after challenge, respectively. Taken together, we show that the DVLP can deliver antigen mRNA specifically to DCs and elicit enhanced immunity.

Results

Design and characterization of a VLP-based SARS-CoV-2 mRNA vaccine

To explore the potential of VLPs as mRNA vaccine carriers, we performed a proof-of-concept study by designing a candidate SARS-CoV-2 mRNA vaccine comprising the full-length spike mRNA and a signal peptide from the human heavy chain of IgE, using a codon-optimized sequence (Fig. 1a). To increase the stability and expression level of the spike mRNA, we also introduced two proline substation mutations (K986P/V987P) in S2 (Fig. 1a)[27]. We and others have previously reported the delivery of CRISPR (clustered regularly interspaced short palindromic repeats) using VLP-mediated efficient genome editing in vitro and in vivo, including in different disease models[28–31]; however, it is unclear whether VLPs can serve as an mRNA vaccine technology. To package the full-length spike mRNA into VLPs, we inserted MS2 stem–loop repeats in the 3′ terminus between the stop codon and the polyA signal. This design allowed the spike mRNA to be internalized via interaction with the MS2 coat protein fused to the N-terminus of lentiviral GagPol polyproteins, which can self-assemble into VLPs (Fig. 1b). As vesicular stomatitis virus G protein (VSV-G)-coated lentiviruses are efficiently taken up by APCs and yield antigens with high immunogenicity[32], we first pseudotyped VLPs with VSV-G by providing the VSV-G envelope glycoprotein-encoding plasmid pMD.2G in the production process. We analysed the morphology of the VLPs using electron microscopy, which showed round particles with a size of approximately 120 nm (Fig. 1c and Supplementary Fig. 1).

To confirm that spike mRNA was packaged into the lentiviral particles, we performed reverse transcription quantitative polymerase chain reaction (RT-qPCR) on the VLPs and normalized the results to those of the traditional lentiviral vector with two RNA copies. We found, on average, three copies of the wild-type spike mRNA and four copies of the mutant mRNA in each VLP (Fig. 1d). Next, we performed RNA immunoprecipitation (RIP) and found that the MS2 stem–loop-containing spike mRNA, but not the stem–loop-null spike mRNA, was efficiently pulled down by the MS2 coat protein, suggesting that the spike mRNA was packaged into VLPs via a specific RNA–cognate protein interaction (Supplementary Fig. 2). To rule out the possibility that the packaged mRNA could undergo reverse transcription, we transduced VLPs into 293T cells and collected DNA for qPCR analysis. Only a background level of DNA was detected, suggesting that the mRNA delivered by the VLPs could not be reverse transcribed (Supplementary Fig. 3). As the spike protein is an envelope protein, we used western blotting analysis of lysates of the VLPs, with an integration-defective lentiviral vector (IDLV) as the control, to determine whether the protein could automatically assemble into the membranes of the VLPs (Fig. 1e). We found successful decoration of the VLPs with both spike proteins, with or without proline mutations. In addition, more of the mutant spike proteins than the wild-type proteins could be loaded, in accordance with the RT-qPCR results. As glycosylation affects the immunogenicity and immunodominance of a vaccine[33], we sought to examine the

Fig. 1 | Design and characterization of a VLP-based SARS-CoV-2 mRNA vaccine. a, Construction of an mRNA-encoding plasmid that transcribes an MS2 stem–loop-containing spike mRNA. The spike mRNA could be packaged into VLPs via the RNA–coat protein interaction during VLP self-assembly. SP, signal peptide; pA, polyadenosine tail; NTD, N-terminal domain; RBD, receptor-binding domain; SD1 and SD2, subdomains 1 and 2; FP, fusion peptide; HR1 and HR2, heptad repeats 1 and 2; TM, transmembrane domain; CT, cytoplasmic tail. **b**, Schematic illustration of the production of the SARS-CoV-2 vaccine using the VLP technology. **c**, Transmission electron microscopy image of a VLP. **d**, The spike mRNA copy number in each VLP. The copy number was determined by absolute quantification using RT-qPCR with normalization to the IDLV–S-mut (two RNA copies per virion) copy number. Data were analysed using unpaired two-tailed Student's *t*-tests. **e**, Western blotting analysis of the spike protein in the virion treated with or without PNGase F. An IDLV was used as a control, with 100 ng p24 for each vector. **f**, Western blotting analysis of spike protein expression. The 293T cells were collected 36 h after transfection or transduction, and 300 ng p24 IDLVs or VLPs was used per well. **g**, Confocal microscopy analysis of spike protein expression. The 293T cells were fixed 36 h after transfection (150 ng plasmid per well) or transduction (150 ng p24 IDLVs or VLPs). Images are representative of three independent biological replicates in one experiment. **h**–**j**, Innate immune response induced by VLPs in THP-1-derived macrophages. Cells were collected for IFNB1 (**h**), ISG15 (**i**) and RIG-I (**j**) analysis by RT-qPCR 6 h after transduction. One hundred and fifty nanograms of p24 per well was used for IDLV–S-mut and VLP–S-mut, and 1.5 μg poly(I:C) per well was used as a positive control. NC, non-infected control; S, spike protein; S-mut, mutant spike protein. Data and error bars represent the mean ± s.e.m.; one-way ANOVA with Dunnett's post hoc test was performed for **h**–**j**; NS, non-significant.

https://doi.org/10.1038/s41551-024-01208-4

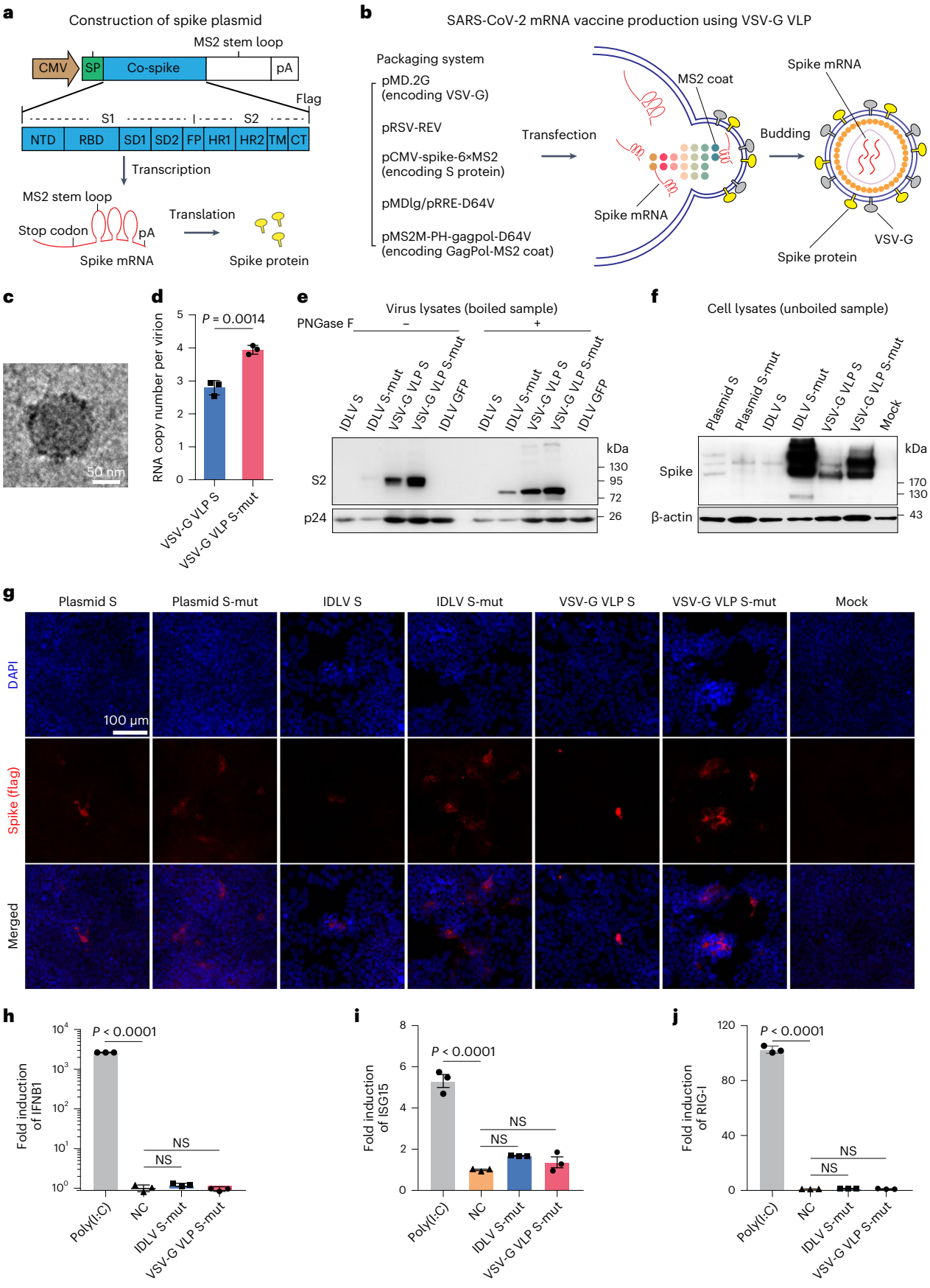

https://doi.org/10.1038/s41551-024-01208-4

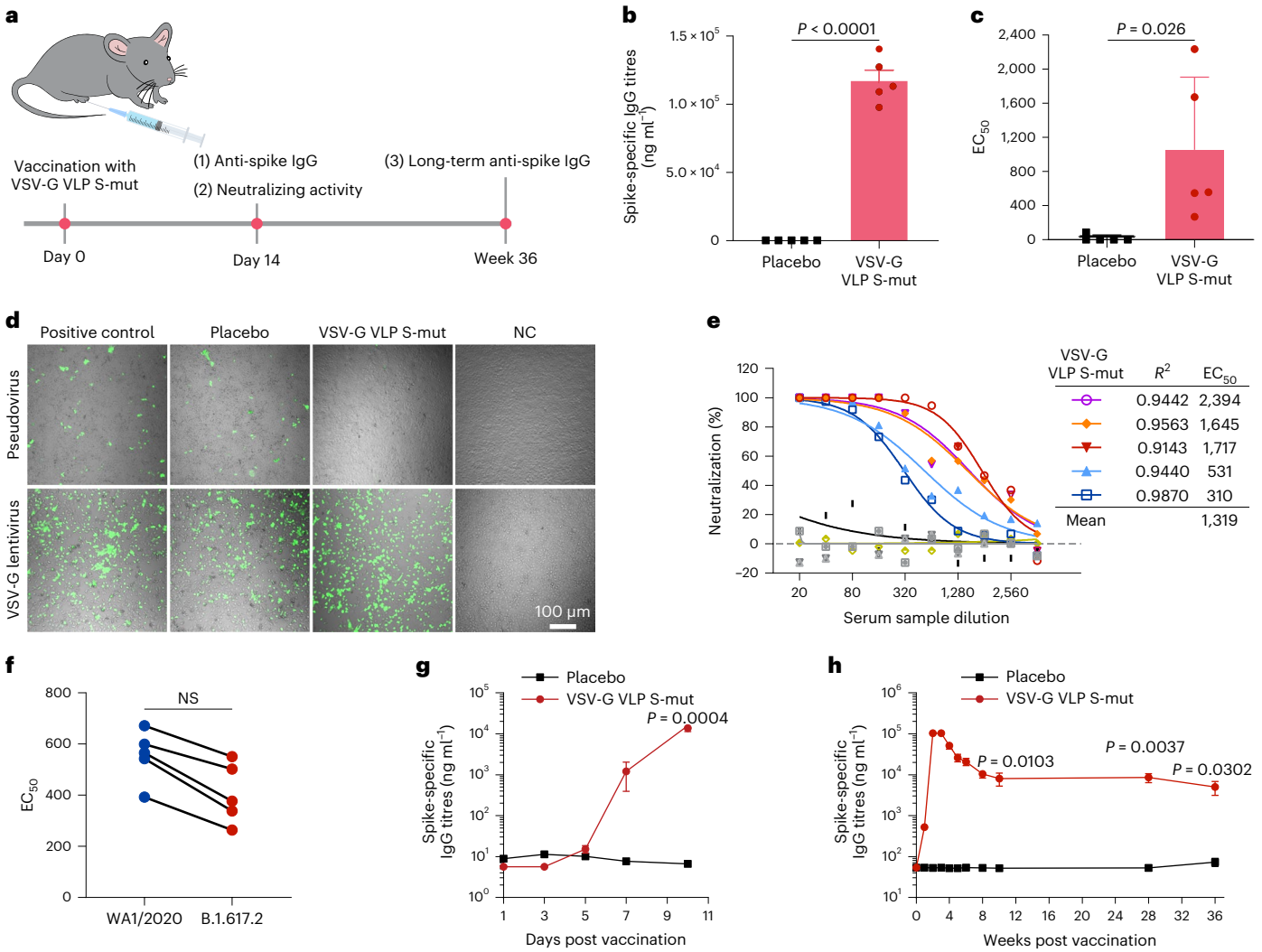

Fig. 2 | VLP–S-mut mRNA induced robust and durable spike-specific antibody responses. a, Schematic illustration of the working plan. Sera were collected for analysis at the indicated time points after footpad vaccination. **b**, ELISA analysis of spike-specific IgG. **c**–**f**, Neutralization activity of vaccinated sera evaluated by luciferase assays (**c** and **f**), confocal microscopy (**d**) and plaque assays (**e**). A firefly-luciferase-encoding SARS-CoV-2 (USA-WA1/2020) pseudovirus (**c** and **f**) and SARS-CoV-2 B.1.617.2 pseudovirus (**f**), a GFP-expressing SARS-CoV-2 pseudovirus (**d**) and live SARS-CoV-2 (USA-WA1/2020) (**e**) were used to transduce Huh-7 (**c**,**d**,**f**) or Vero E6 cells (**e**). Images are representative of three independent biological replicates in one experiment (**d**). Positive control, spike–pseudovirus-infected Huh-7 cells; placebo, PBS-treated mice; NC, non-infected control, Huh-7 cells without virus infection. In **f**, $P = 0.0625$ ($n = 5$ mice). **g**,**h**, Short-term (**g**) and long-term (**h**) changes in antibody concentrations after vaccination. $n = 5$ mice in **g**. $n = 10$ mice in **h**, except for weeks 28 and 36, where $n = 5$ mice. Mice were immunized with 2 μg (**b**–**f**) or 1.5 μg (**g**–**h**) p24 VSV-G VLP–S-mut. Data and error bars represent the mean ± s.e.m. Unpaired two-tailed Student's *t*-tests (**b** and **c**) or two-tailed Wilcoxon matched-pairs signed-rank tests (**f**) were performed.

glycosylation status of the spike protein on the surface of the VLPs. Notably, mass spectrometric analysis showed that the S2 bands shifted downwards after Peptide:N-glycosidase F (PNGase F) treatment, indicating that the spike proteins on the VLPs were modified by N-linked glycosylation, mimicking the characteristics of SARS-CoV-2 (Fig. 1e)[34].

As the VLPs were decorated by both the spike and VSV-G proteins, we examined whether the spike mRNA in the VLPs could be delivered intracellularly using VSV-G by transducing 293T cells to which SARS-CoV-2 was inaccessible unless supplemented with human angiotensin-converting enzyme 2 (hACE2)[35]. The 293T cells were then collected 36 h after transduction for western blotting (Fig. 1f). We found two major bands for the spike protein, which were likely glycosylated full-length singlet spike proteins and their dimeric/trimeric forms (Fig. 1f). As the spike protein detected in the cytosol may be either from the envelope proteins decorating the surfaces of the VLPs or the translation of spike mRNA, we cloned a truncated spike construct from which we removed the transmembrane domain and cytoplasmic tail to abolish its self-assembly on the surface of the VLPs (Supplementary Fig. 4a). First, we performed western blotting analysis of viral lysates, which showed that the truncated spike protein failed to be loaded on the VLPs (Supplementary Fig. 4b). Second, we transduced the VLPs into 293T cells and performed western blotting using the cell lysates. We could still detect the truncated spike protein, indicating that the mRNA in the VLPs could be successfully translated into proteins in the target cells (Supplementary Fig. 4c). In addition, confocal microscopy analysis confirmed that the VLPs successfully delivered the spike protein to 293T cells with an efficiency comparable to the IDLV (Fig. 1g and Supplementary Fig. 5). Western blotting and confocal microscopy analyses consistently showed that the mutant spike antigens outperformed the wild-type spike antigens. Therefore, we chose the mutant spike protein for in vivo evaluations.

As mRNA transcribed in vitro for LNP delivery is recognized by intracellular RNA sensors, unless chemically modified[36,37], we examined the innate immune properties of the mRNA-carrying VLPs.

Using Tohoku Hospital Pediatrics-1 (THP-1)-derived macrophages as a model of nucleic acid sensing, we found no significant changes in the expression levels of interferon beta 1 (IFNB1), IFN-stimulated genes (ISG15) or retinoic acid-inducible gene I (RIG-I) 6 h after transduction (Fig. 1h–j). To confirm this finding, we analysed the innate immune response in more cell types, namely, murine DC2.4 cells, primary human T cells, primary human peripheral blood mononuclear cells (PBMCs) and primary murine hepatocytes and extended the detection time points up to 72 h. Moreover, we evaluated mRNA from different sources by comparing in vitro transcribed (IVT) unmodified mRNA, IVT modified mRNA and VLP-carried mRNA (Supplementary Fig. 6). We found that both polyinosinic:polycytidylic acid (poly(I:C)) and IVT unmodified mRNA induced a strong type I innate immune response in all cell types and time points examined, whereas chemical modification of the IVT mRNA significantly reduced the innate immune response. Notably, the VLP-carried mRNA did not or only slightly upregulated the innate immune response at late time points (Supplementary Fig. 6). This may have been caused by the carryover of plasmids or genomic DNA from the 293T producer cells. Together, our data suggested that the spike mRNA in the VLPs had low immunogenicity, likely because this mRNA was produced intracellularly and shared the same modifications as other endogenous mRNAs.

VLPs containing mutant S mRNA induced robust and durable spike-specific humoral responses

To evaluate the potential of VLP-encapsulated mRNA as a vaccine technology, we vaccinated C57BL/6J mice ($n = 5$) with 2 μg p24 VLP carrying a mutant spike mRNA (VLP–S-mut) via footpad injection (Fig. 2a). Two weeks later, we performed an enzyme-linked immunosorbent assay (ELISA) using sera from mice as a source of spike-specific IgG. As shown in Fig. 2b, we observed significant elicitation of spike-specific IgG. To evaluate the level of neutralizing antibodies, we performed a well-established pseudovirus neutralization assay using spike-pseudotyped HIV encoding firefly luciferase[38]. We found that a single injection of VLP–S-mut was sufficient to induce a potent neutralizing immune response (Fig. 2c). To confirm the neutralizing activity of sera from vaccinated mice, we transduced Huh-7 cells with a spike-pseudotyped lentiviral vector encoding green fluorescent protein (GFP). We found that pre-incubation with 1:40-diluted sera from vaccinated mice almost completely abolished the fluorescence, whereas transduction with a VSV-G-pseudotyped lentivirus was not affected by the spike-specific neutralizing activity (Fig. 2d). Importantly, the induction of antibodies with high neutralization titres was demonstrated using live SARS-CoV-2, with an average half-maximal effective concentration (EC_{50}) titre of 1,319 (Fig. 2e). In addition, we analysed the neutralizing activity of the VLP–mRNA vaccine against the B.1.617.2 strain pseudovirus, which showed a non-significant tendency towards a reduced EC_{50} titre compared with the SARS-CoV-2 (USA-WA1/2020) strain pseudovirus (Fig. 2f).

To evaluate the dynamic changes in VLP–mRNA-induced spike-specific antibodies, we performed a short-term follow-up experiment starting from 1 day post vaccination and a long-term follow-up experiment up to 9 months after vaccination. Spike-specific IgG was not evident on day 1, 3 or 5 but was detected from day 7 (Fig. 2g). In addition, the IgG response was further enhanced by a booster injection (Supplementary Fig. 7). In the long-term follow-up experiment, we found that a single-dose vaccination induced a durable spike-specific IgG response, which was maintained at a high level up to 36 weeks post immunization (Fig. 2h). Notably, no significant weight loss was found after vaccination, suggesting the safety of the VLP–mRNA vaccine (Supplementary Fig. 8). Interestingly, administration of the VLP–mRNA vaccine via the intranasal route elicited spike-specific IgA in the lung, suggesting that this vaccine technology may also be used as an intranasal vaccine to induce mucosal immunity to block SARS-CoV-2 infection at the first contact site (Supplementary Fig. 9).

To dissect the linear epitope profiles of the spike-specific antibodies in VLP–mRNA-vaccinated mice, we used a peptide microarray containing short peptides covering the full length of the spike protein[39–41]. We found varying intensities of signals corresponding to specific spike peptides in the vaccinated group, while no signal was observed for placebo-treated mice (Supplementary Fig. 10a). Next, we quantified the signal intensity for antibodies against the S1 domain and receptor-binding domain (RBD) and found that the sera from vaccinated mice elicited significantly higher signals for both antibodies, suggesting the presence of high amounts of S1- and RBD-specific IgG in vaccinated mice (Supplementary Fig. 10b). To visualize the panorama of epitopes, we constructed a heat map for all six vaccinated mice (Supplementary Fig. 10c). Notably, although the epitopes were highly diverse, three epitopes, that is S2-22, S2-76 and S2-83, were shared by 66.7% of the vaccinated mice (Supplementary Fig. 10d,e). Interestingly, the S2-22 epitope also appeared in the majority of convalescent mice[39]. Moreover, the S2-76 and S2-83 epitopes are conserved among different coronaviruses (Supplementary Fig. 11).

DVLP–S-mut mRNA elicited an enhanced immune response in vivo

To target the VLPs specifically to DCs, we used an engineered Sindbis virus glycoprotein (designated SV-G) which could recognize DC-SIGN, a surface protein of DCs, to replace the broad tropic protein VSV-G (Fig. 3a). We first analysed the size of SV-G VLPs using a particle size analyser (Malvern Panalytical) and found that the VLPs and the lentiviral vector had similar diameters (Supplementary Fig. 12). Next, we quantified the copy number of the mutant spike mRNA in each SV-G VLP using RT-qPCR and found that it was 3.5 copies on average (Supplementary Fig. 13). We then verified the tropism of the SV-G-pseudotyped VLPs in vitro by transducing DC2.4 and HeLa cells with 100 ng p24 SV-G VLP–GFP or VSV-G VLP–GFP. The cells were collected at 3 days post infection (d.p.i.) and analysed by flow cytometry. SV-G VLPs efficiently transduced into DCs which expressed high levels of the SV-G receptor, DC-SIGN (63% GFP^+ cells), whereas SV-G VLPs transduced into only 22.8% of non-DCs (HeLa cells), in contrast to VSV-G VLPs, indicating that SV-G VLPs had preferable tropism of DCs (Fig. 3b).

Fig. 3 | DVLP–S-mut mRNA vaccine enhanced spike-specific immune response. a, Illustration of the production of the DC-specific VLP–mRNA vaccine. **b**, Evaluation of the DC specificity of SV-G-pseudotyped VLPs. One hundred nanograms of p24 GFP-carrying VLP–S-mut pseudotyped by SV-G, VLP or VSV-G was transduced into 4×10^4 DC2.4 or HeLa cells. The transduction efficiency was measured by flow cytometry 3 days later. **c**, Comparison of the transduction efficiency of SV-G- and VSV-G-pseudotyped VLPs in mBMDCs. mBMDCs were infected with VLPs (400 or 600 ng p24) and analysed for GFP^+ and $CD11c^+$ cells by flow cytometry 3 days after transduction. **d**,**e**, DC activation analysis by RT-qPCR. BMDCs were infected with 400 or 600 ng p24 SV-G VLP or VSV-G VLP. mRNA was extracted for CD80 (**d**) and CD86 (**e**) detection 3 days after transduction. **f**, Flowchart of the analysis of the VLP–mRNA-elicited immune response. **g**,**h**, Analysis of the size of lymph nodes. Seven hundred and fifty nanograms of p24 VLP was injected into the right footpad of C57BL/6J mice ($n = 6$), and PBS was injected into the left footpad as a control. **g**, Representative images of the popliteal lymph node (PLN) were taken 3 days after injection. **h**, The volume of the PLNs. **i**,**j**, ELISA analysis of spike-specific (**i**) and p24-specific (**j**) IgG in sera collected 14 days post immunization. Each mouse ($n = 4$) was injected with 1.5 μg p24 VLP (S-mut). **k**–**m**, Quantification of IFN-γ (**k**), TNF-α (**l**) and IL-2 (**m**) spot-forming cells isolated from the spleen after stimulation with the spike peptide pool. Representative ELISpot images on the left are three independent biological replicates from one experiment. Data and error bars represent the mean ± s.e.m. Unpaired two-tailed Mann–Whitney tests (**i**,**j**), paired two-tailed Wilcoxon tests (**h**) and unpaired two-tailed Student's *t*-tests (**b**–**e**,**k**–**m**) were performed.

https://doi.org/10.1038/s41551-024-01208-4

We next characterized the performance of SV-G VLPs in DCs using mouse bone-marrow-derived DCs (mBMDCs). We found that the SV-G VLPs showed higher transduction efficiency in mBMDCs than the VSV-G control at varied dosages (Fig. 3c). To evaluate the immunogenicity of the VLPs, we transduced mBMDCs with differently pseudotyped VLPs, using poly(I:C) as a control. In accordance with the THP-1 macrophage study, we found that the VLPs had low immunogenicity, with only a slight induction of IFNB1 24 h after the transduction of SV-G VLPs

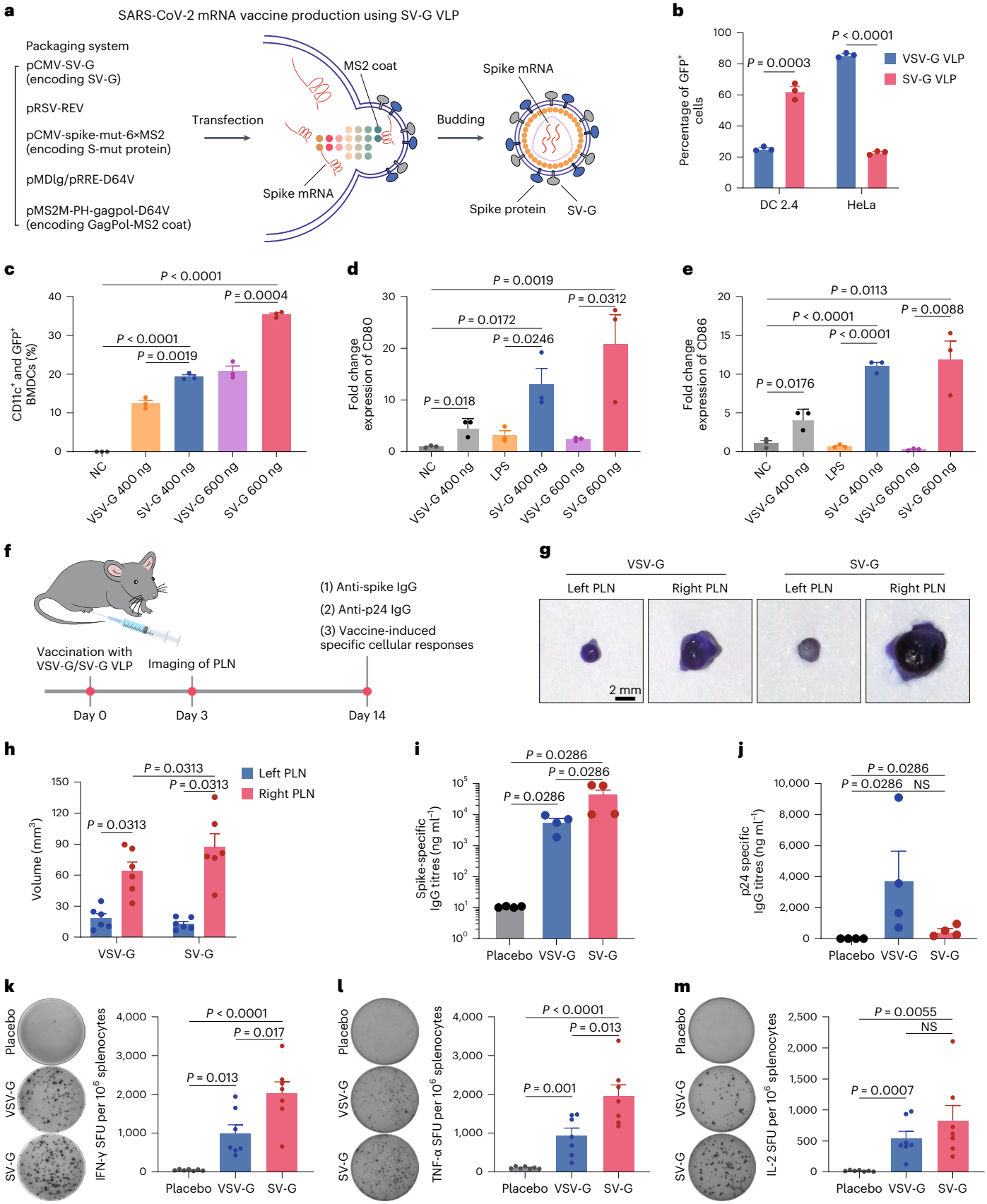

https://doi.org/10.1038/s41551-024-01208-4

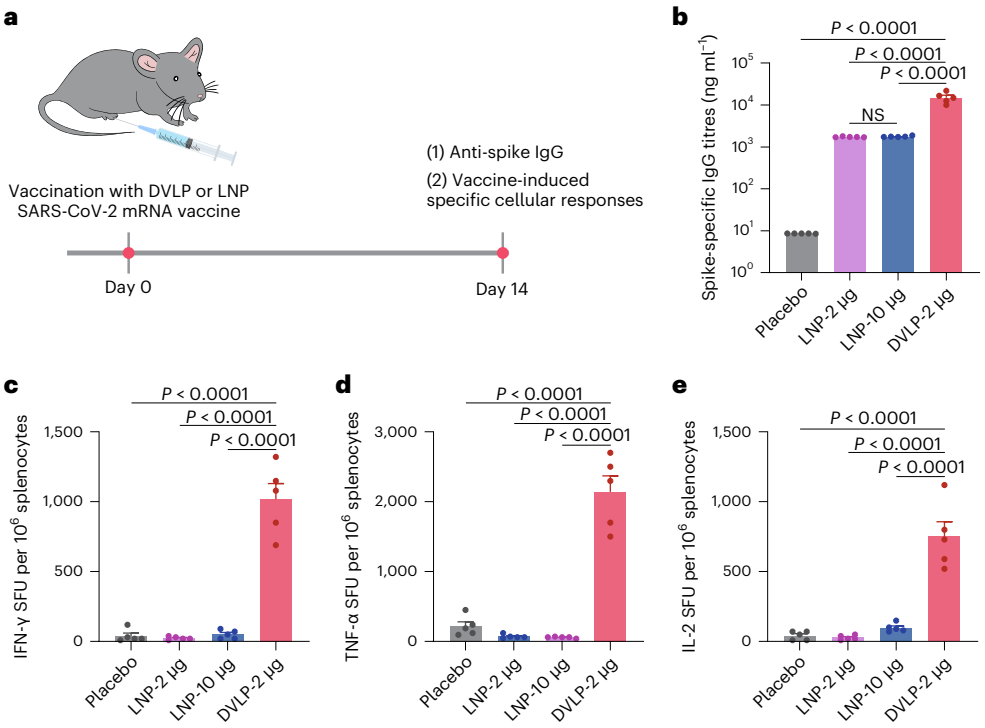

Fig. 4 | DVLP–S-mut mRNA improved spike-specific humoral and T-cell responses compared with LNP–mRNA. a, Scheme illustration of DVLP and LNP vaccination. Mice were vaccinated with DVLPs (2 μg p24) or LNPs (2 μg or 10 μg) via footpad injection. The sera and spleen were collected 12 days after vaccination for further analysis. **b**, ELISA analysis of spike-specific IgG. **c**–**e**, Quantification of IFN-γ (**c**), TNF-α (**d**) and IL-2 (**e**) spot-forming units (SFU) isolated from the spleen after stimulation with a spike peptide pool ($n = 5$ mice). Data and error bars represent the mean ± s.e.m. Unpaired two-tailed Student's *t*-tests were performed.

(Supplementary Fig. 14). We further examined whether the targeted transduction could increase CD80/CD86 expression levels, which would allow stronger T-cell-receptor engagement and more potent T-cell activation. A qPCR assay revealed that incubation with SV-G VLP–GFP significantly enhanced the expression levels of CD80 and CD86 (Fig. 3d,e). Notably, SV-G VLPs significantly outperformed both lipopolysaccharide and the non-specific VSV-G VLPs. Taken together, our results suggested that SV-G VLPs were specifically and efficiently transduced into DCs and induced DC maturation. Therefore, they were designated as DVLPs.

To test whether SV-G-pseudotyped VLPs could improve the immune response in vivo, we compared SV-G and VSV-G pseudotyping of VLPs in mice (Fig. 3f). We injected 750 ng SV-G or VSV-G VLPs into the right footpad of C57BL/6J mice ($n = 6$) and found a significantly greater enlargement of lymph nodes in response to SV-G VLPs than VSV-G VLPs or phosphate-buffered saline (PBS) controls on day 3, indicating that the administration of DVLPs enhanced the trafficking of DCs to nearby lymph nodes (Fig. 3g,h). Next, we directly compared the humoral and cellular immune responses induced by SV-G- and VSV-G-pseudotyped VLPs in vivo (Fig. 3i–m). C57BL/6J mice ($n = 4$) were immunized with 2 μg p24 SV-G VLP–S-mut or VSV-G VLP–S-mut via footpad injection. Humoral immune responses were evaluated by ELISA at 14 days post immunization. We found that the DC-targeting SV-G VLPs significantly increased the levels of spike-specific IgG and p24-specific IgG (Fig. 3i,j). Furthermore, we set out to evaluate the spike-specific T-cell responses for both the DC-targeting and non-targeting VLP–mRNAs. Although we found that both VLP–mRNAs elicited a strong T-cell immune response, as shown by IFN-γ, tumour necrosis factor-alpha (TNF-α) and interleukin-2 (IL-2) enzyme-linked immunosorbent spot (ELISpot) assays, vaccination with the SV-G VLP–mRNA induced significantly higher levels of IFN-γ and TNF-α than the VSV-G VLP–mRNA, as indicated by more spot-forming units (Fig. 3k–m).

DVLP–S-mut mRNA improved the spike-specific immune response compared with LNPs

To compare the immune responses to the DVLP–mRNA vaccine and the LNP–mRNA vaccine, we generated LNPs according to a previous publication and synthesized chemically modified mRNA encoding the SARS-CoV-2 spike by in vitro transcription before combining the two components (Fig. 4a)[42,43]. Twelve days after footpad injection of the two nanoparticles, we found that both elicited a significant spike-specific antibody response, but the response to 2 μg p24 DVLP was much greater than to LNP at both the 2 μg and 10 μg dosages (Fig. 4b).

To evaluate spike-specific T-cell immune responses, the splenocytes of vaccinated mice were collected and stimulated with a SARS-CoV-2 spike peptide pool 12 days after vaccination, and cytokine-producing T cells were quantified using ELISpot assays. After stimulation with peptides, we detected a significant increase in the number of T cells producing IFN-γ, TNF-α and IL-2 in mice vaccinated with the DVLP–S-mut mRNA (Fig. 4c–e). However, the spike-specific T-cell response was inefficient in mice vaccinated with the non-targeting LNP–mRNA, as shown by IFN-γ, TNF-α and IL-2 spots, which is in agreement with a previous report[44]. This result suggested that DVLP–mRNA may improve humoral and cellular immune responses compared with LNP–mRNA.

In vivo characterization of the biodistribution and DC-targeting capability of DVLPs

To reveal the potential mechanism that contributes to the improved performance of DVLPs, we sought to directly compare LNPs, VSV-G VLPs and DVLPs at both the mRNA and protein levels (Fig. 5a). We found the DVLP-delivered spike mRNA was significantly enriched in the lymph nodes after footpad vaccination compared with the non-specific VSV-G VLPs, although the two VLPs resulted in similar quantities of mRNA at the injection sites (Fig. 5b–d). Next, to assess whether the

https://doi.org/10.1038/s41551-024-01208-4

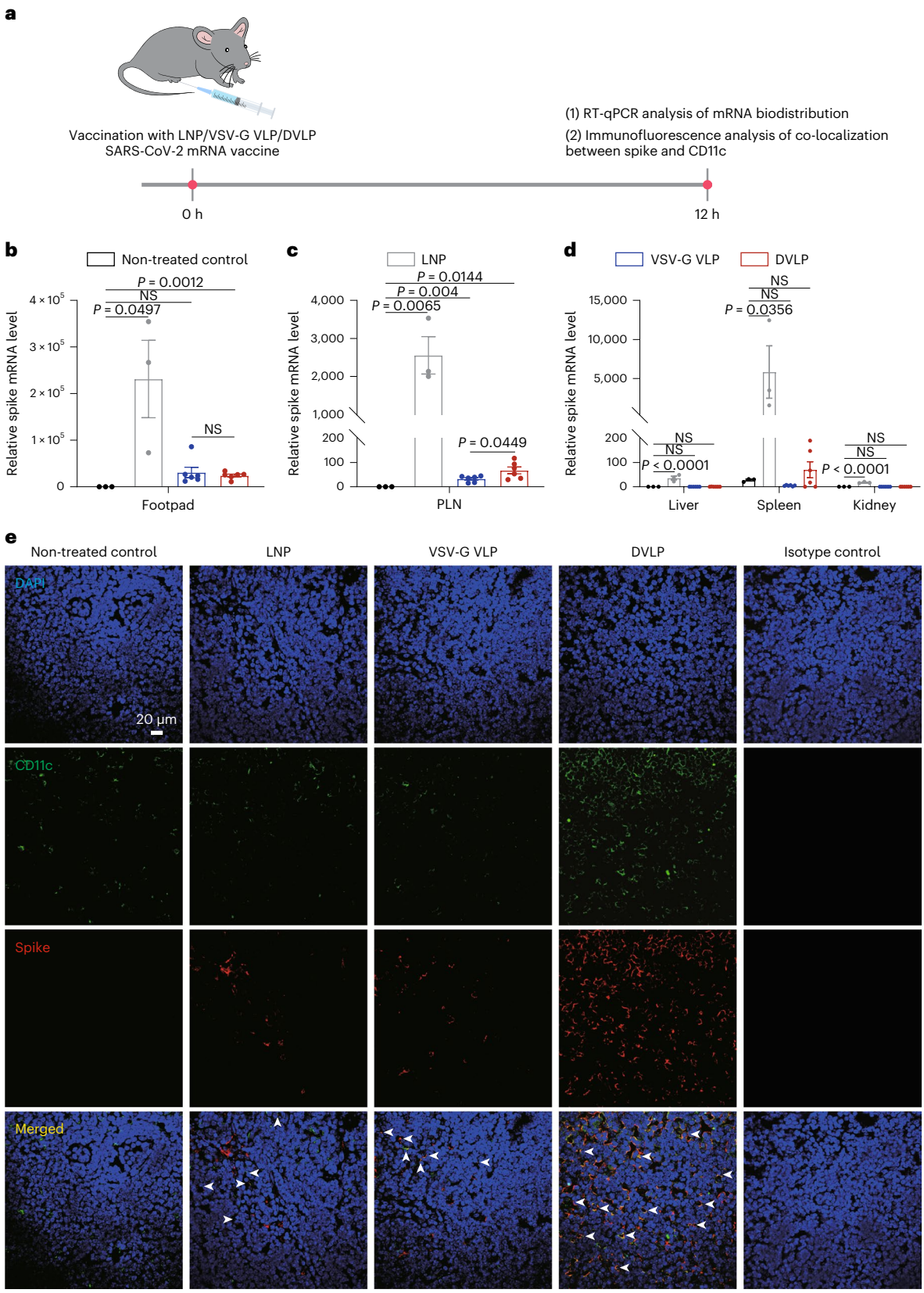

Fig. 5 | In vivo characterization of the biodistribution and DC-targeting capability of DVLPs. a, Experimental workflow. **b**–**d**, In vivo biodistribution of LNPs, VSV-G VLPs and DVLPs at the injection sites (**b**), in the popliteal lymph nodes (**c**) and in the liver, spleen and kidney (**d**) after vaccination via footpad injection. Spike mRNA was detected by RT-qPCR 12 h after injection. Non-infected control and LNP spike mRNA, $n = 3$ mice; VSV-G VLP–spike mRNA and DVLP–spike mRNA, $n = 6$ mice. **e**, Immunofluorescence analysis of the co-localization of DVLPs and DCs. The PLNs were collected 12 h after footpad injection of the vaccines. Each image is representative of three mice from one experiment. The white arrowheads indicate the co-localization of spike protein with CD11c, a marker protein of DCs. Data and error bars represent the mean ± s.e.m. For **b** (footpad) and **c** (PLN), unpaired two-tailed Student's *t*-tests were performed; for **d** (liver, spleen and kidney), two-tailed one-way ANOVA was performed.

https://doi.org/10.1038/s41551-024-01208-4

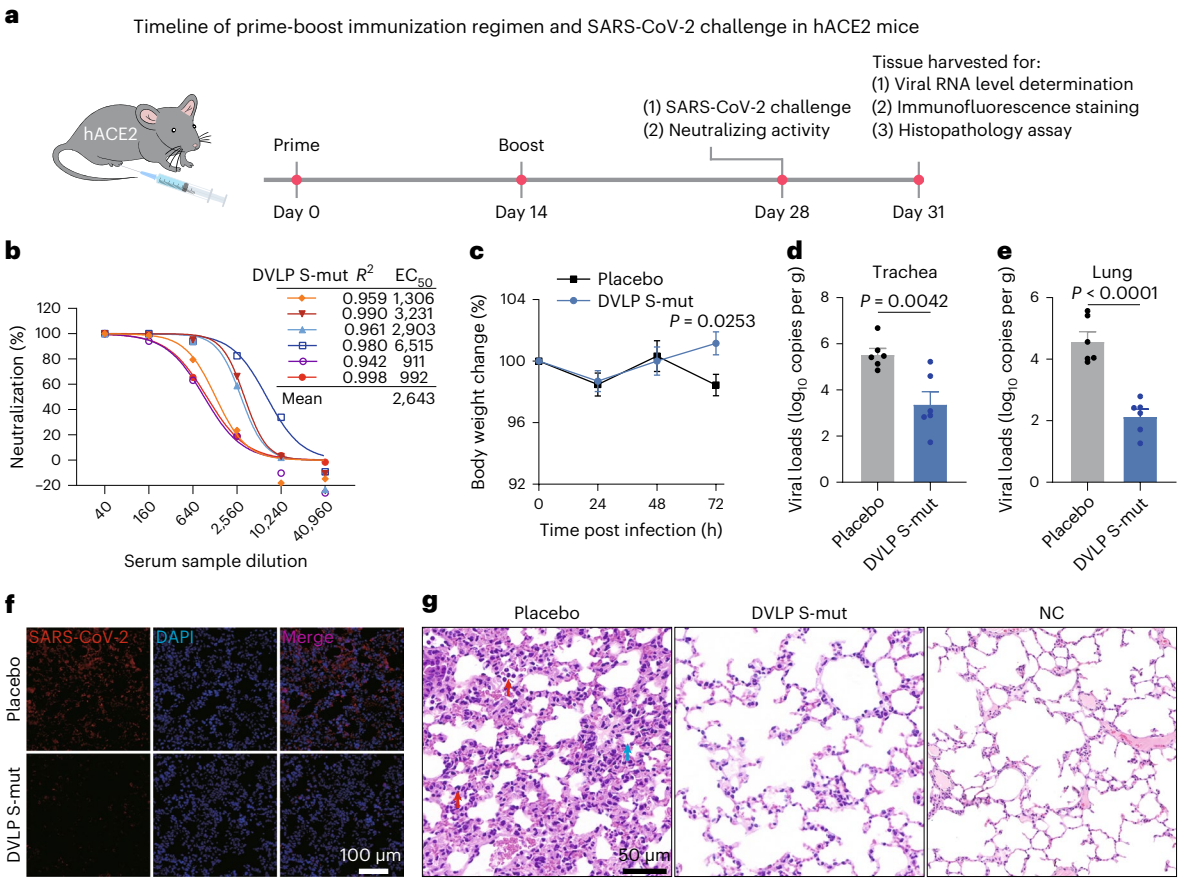

Fig. 6 | The DVLP–S-mut mRNA vaccine efficiently protected hACE2-transgenic mice from SARS-CoV-2 challenge. a, Schematic illustration of the vaccination and challenge. Mouse footpads were injected with 1.5 μg p24 DVLPs or 50 μl PBS, and a booster injection was administered 14 days after the prime immunization. The mice were challenged with a 10^5 50% tissue culture infectious dose of SARS-CoV-2 by intranasal administration 14 days after booster immunization. All mice were euthanized at 3 d.p.i. **b**, The neutralization activity of vaccinated sera against live SARS-CoV-2 (nCoV-2019 BetaCoV/Wuhan/WIV04/2019). **c**, The percentage weight change of the mice after infection. **d**,**e**, Viral loads in the trachea (**d**) and lungs (**e**) detected by RT-qPCR. **f**, Confocal analysis of SARS-CoV-2 in the lungs. **g**, Lung histopathology analysis by H&E staining (red arrow, inflammatory cell infiltration; blue arrow, alveolar destruction). In **f** and **g**, each image is representative of a group of four mice. Data and error bars represent the mean ± s.e.m. In **c**–**e**, unpaired two-tailed Student's *t*-tests were performed.

DVLPs were able to target DCs in vivo, we analysed the localization of spike and CD11c proteins in the popliteal lymph node near the injection site 12 h after vaccination. We found that most of the spike and CD11c signals were co-localized in cells after DVLP administration, whereas only a small percentage of spike$^+$ D were also CD11c$^+$ in cells after LNP and VSV-G VLP administration (Fig. 5e). Notably, the DVLP group showed the greatest number of spike$^+$ cells in the lymph nodes (Fig. 5e), although the amount of DVLP-delivered mRNA was markedly less than the amount of LNP-delivered mRNA at both the injection site and the lymph nodes (Fig. 5b,c). Moreover, we analysed spike and CD11c expression in the footpads. Unlike in the lymph nodes, we found only a few CD11c$^+$ cells distributed sparsely in the injection sites of all vaccinated mice, and CD11c was expressed at low levels (Supplementary Fig. 15). Although we were able to find cells that co-expressed spike and CD11c after all vaccine treatments, these may have been resident CD11c$^+$ macrophages, as the transduced DCs may have migrated to the lymph nodes (Supplementary Fig. 15). Taken together, our data suggested that the DVLPs were preferably transduced into DCs in vivo, and the spike-loaded DCs efficiently migrated to lymph nodes.

In addition, we assessed whether VLPs were biocompatible and tolerated in vivo. The liver, kidney and spleen were collected for histopathological analysis 7 days after vaccination. We did not find apparent inflammatory immune cell infiltration, cell necrosis or other signs of tissue damage (Supplementary Fig. 16a). Next, we performed alanine transaminase (ALT) and blood urea nitrogen (BUN) tests to evaluate liver and kidney function, respectively. No upregulation of ALT or BUN concentrations was found after LNP, VSV-G VLP or DVLP treatments, indicating that all tested vaccines were tolerated in mice, without causing significant systemic toxicities (Supplementary Fig. 16b,c).

The DVLP–S-mut mRNA vaccine protected hACE2-transgenic mice from SARS-CoV-2 challenge

To evaluate whether the DVLP–mRNA vaccine was able to protect mice from live SARS-CoV-2, we challenged hACE2-transgenic mice, which support efficient SARS-CoV-2 replication, with live virus[44]. To acquire optimal efficacy, hACE2-transgenic mice ($n = 6$ mice per group) were dosed twice with 1.5 μg of the p24 VLP–mRNA vaccine (Fig. 6a). The mice were then inoculated by intranasal infection with 10^5 plaque-forming units (p.f.u.) of SARS-CoV-2 (nCoV-2019 BetaCoV/Wuhan/WIV04/2019) 2 weeks after the booster vaccination. We detected high concentrations of neutralizing anti-SARS-CoV-2 antibodies on day 28, with a mean EC_{50} value of 2,643 (Fig. 6b). The weight of the mice was monitored daily before euthanasia at 3 days post challenge. We found that the vaccinated mice kept growing, but the unvaccinated mice lost an average of 2% of their body weight (Fig. 6c). Next, we analysed the viral RNA levels and found a significant reduction in viral load in the lungs and trachea of DVLP-vaccinated mice (Fig. 6d,e).

https://doi.org/10.1038/s41551-024-01208-4

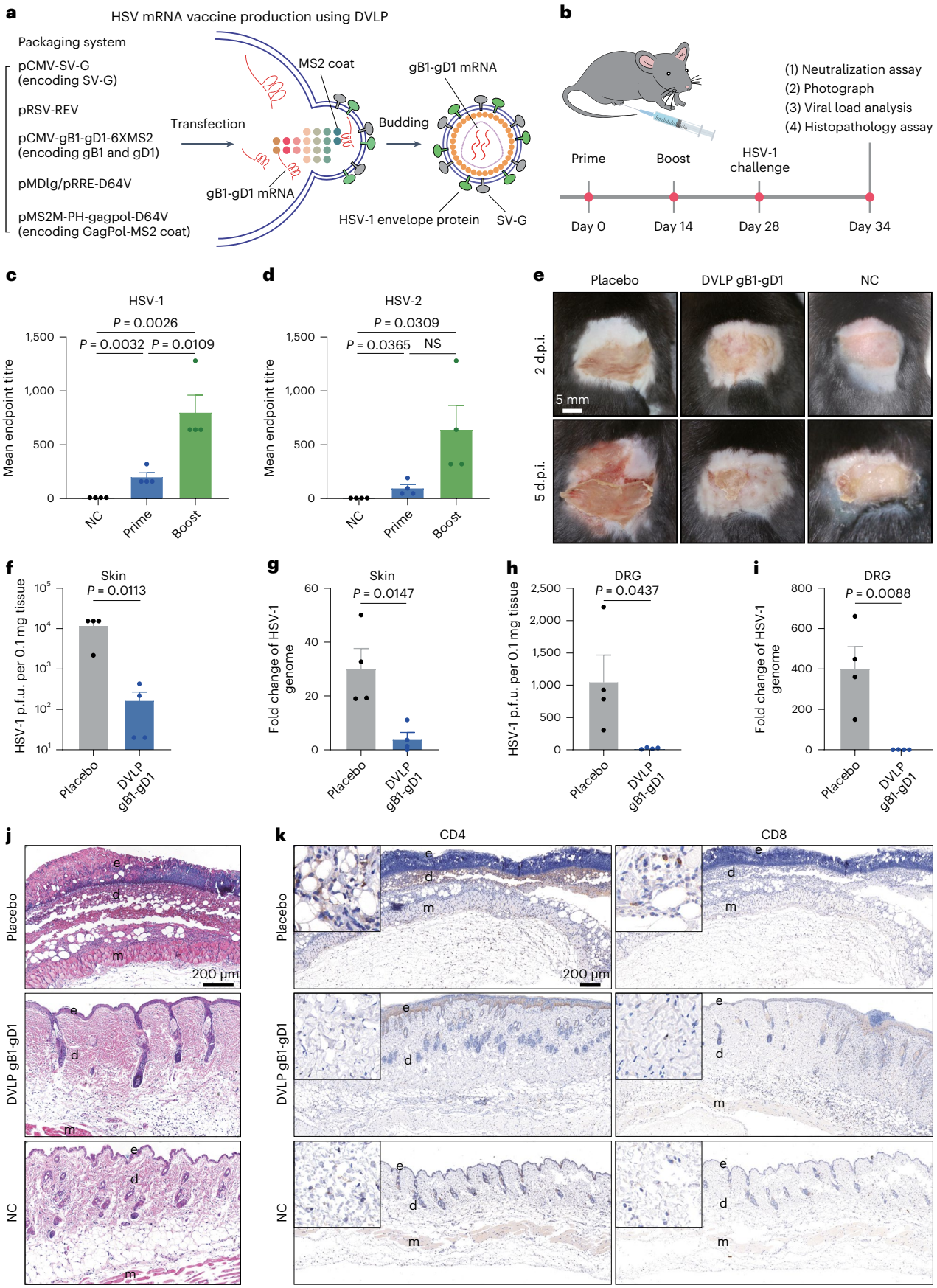

Fig. 7 | The DVLP-mediated delivery of *gB1* and *gD1* mRNA efficiently protected mice from HSV-1 infection. a, Schematic illustration of the production of the DVLP–gB1–gD1 mRNA vaccine. **b**, Flowchart of the analysis of the efficacy of DVLP–gB1–gD1 mRNA vaccination against HSV-1 infection. Six-week-old C57BL/6J mice were immunized with 2 μg of the p24 VLP–mRNA vaccine on day 0 and day 14 ($n = 4$ mice). **c**,**d**, Neutralization activity against live HSV-1 (**c**) and HSV-2 (**d**) ($n = 4$ mice). **e**, Representative images of the skin at 2 d.p.i. and 5 d.p.i. Each image is representative of four mice from one experiment. **f**,**g**, Plaque assays (**f**) and qPCR (**g**) analysis of HSV-1 replication in the skin at 6 d.p.i. **h**,**i**, Plaque assays (**h**) and qPCR (**i**) analysis of HSV-1 replication in the DRG at 6 d.p.i. **j**, H&E staining analysis of skin histopathology at 6 d.p.i. **k**, Immunohistochemical analysis of $CD4^+$ and $CD8^+$ T-cell infiltration in the skin at 6 d.p.i. e, epidermis; d, dermis; m, muscle. In **e**, **j** and **k**, each image is representative of four mice from one experiment. Data and error bars represent the mean ± s.e.m. Unpaired two-tailed Student's *t*-tests were performed.

To analyse the efficacy of VLP–mRNA vaccination for lung protection, we conducted immunofluorescence microscopy, which showed that SARS-CoV-2 was barely detectable in the lungs of vaccinated mice in contrast to placebo-treated mice (Fig. 6f). Moreover, we performed haematoxylin and eosin (H&E) staining to analyse the pathology of SARS-CoV-2-infected mice, which showed that the control mice had alveolar epithelial cell hyperplasia, vascular endothelial cell proliferation, local pulmonary alveoli shrinkage and infiltration of inflammatory cells in the lung interstitium (Fig. 6g). By contrast, vaccinated mice showed attenuation of the inflammatory response, with only mild perivascular and alveolar infiltration of inflammatory cells observed in very few areas (Fig. 6g). Together, these results indicate that the DVLP–mRNA vaccine mediated efficient protection against live SARS-CoV-2 infection and prevented the inflammatory reaction 3 days after challenge.

The DVLP-encapsulated *gB1*–*gD1* mRNA vaccine protected mice from HSV-1 challenge

To evaluate the flexibility of DVLPs as a vaccine technology, we designed an HSV-1 mRNA vaccine by incorporating HSV-1 *gB1* and *gD1* mRNA into SV-G-pseudotyped VLPs (Fig. 7a). We challenged depilated mice with 10^7 p.f.u. of HSV-1 17syn$^+$ by adding 10 μl to abraded skin 14 days after prime–boost vaccination (Fig. 7b). Prime vaccination significantly induced the production of neutralizing IgG against HSV-1, while the second vaccination further increased the neutralizing antibody titres (Fig. 7c and Supplementary Fig. 17). Interestingly, although the gB and gD antigens were derived from HSV-1, we detected cross-neutralizing activity against HSV-2 antigens, suggesting that the vaccine may also be functional against HSV-2 infection (Fig. 7d). After challenging the skin with live HSV-1, vaccinated mice did not show the typical symptoms of disease progression ($n = 4$ mice), in contrast to the placebo-treated mice, which showed mild zosteriform lesions at 2 d.p.i. and hunched posture, abnormal gait and severe zosteriform lesions at 5 d.p.i. (Fig. 7e).

To evaluate whether this vaccine blocked the transmission of HSV-1 from the skin to the peripheral nervous system, skin and dorsal root ganglion (DRG) samples were collected at the time of euthanasia and examined for the presence of the HSV-1 genome. The viral load was significantly reduced in the skin tissues of the vaccinated group compared with the placebo group, as determined by plaque assays and viral genome analysis (Fig. 7f,g). Remarkably, we found almost undetectable levels of virus in the DRG of vaccinated mice in both assays, indicating strong neuronal protection by DVLP–*gB1*–*gD1* mRNA vaccination (Fig. 7h,i). To assess the tissue structure after vaccination and virus challenge, we conducted H&E staining of the skin, which was found to be well preserved in vaccinated mice but showed a thickened epidermis and a seriously damaged dermis in unvaccinated mice (Fig. 7j). Next, we performed immunohistochemistry to compare the local immune response in the skin of infected mice and found apparent enrichment of $CD4^+$ cells, but not $CD8^+$ cells, in the skin of unvaccinated mice after HSV-1 challenge (Fig. 7k). In addition, a large number of neutrophils infiltrated the dermis of unvaccinated mice, which was not evident in vaccinated mice or non-infected control mice (Fig. 7k). Taken together, these findings show that the DVLP–mRNA vaccine effectively protected mice from live HSV-1 infection.

Discussion

Effective vaccines for preventing or curing viral infections, such as HSV-1, HSV-2 and HIV, as well as cancer remain an unmet need. DCs are the most potent APCs and an important cell type to induce effective and durable protective T-cell immunity and a humoral immune response to block pathogens or attack cancer cells[45]. The clinically approved mRNA vaccines are based on LNPs, which are internalized passively by a diverse range of somatic cells, including muscle cells, B cells, $CD4^+$ T cells and tissue-resident or recruited APCs[46]. The alternative approach is to deliver an mRNA vaccine specifically to DCs. In this study, we developed a DC-targeting mRNA-vaccine technology by incorporating mRNA into VLPs. We found that the DVLP–mRNA vaccine significantly improved both the humoral and T-cell immune response compared with the non-specific control vaccines. Moreover, the DVLP–mRNA vaccines protected mice from viral infections in both live SARS-CoV-2 and live HSV-1 infection models.

Our DVLP vaccine technology is derived from an IDLV. IDLVs have been reported to induce strong, long-lasting cellular and humoral immune responses[47]. Moreover, lentiviral vectors have negligible inflammatory properties, and, unlike many other viral vectors, there is no pre-existing vector-specific immunity in most humans[48]. In addition, IDLVs can be retargeted to DCs by surface engineering. Owing to such advantages, IDLVs have been used in clinical trials against HIV and cancers[47,48]. Recently, IDLVs have been administrated intranasally in preclinical animal models and have elicited efficient protection against SARS-CoV-2 infection[49]. However, IDLVs face two intrinsic challenges: the viral DNA has potential insertional risks, and the presence of SAMHD1, a cellular enzyme that depletes intracellular deoxynucleoside triphosphates and blocks reverse transcription, may limit antigen presentation[50]. Although DVLPs retain the advantages of IDLVs, they deliver mRNA, which does not cause insertional mutagenesis. Moreover, as no reverse transcription step is required, they escape negative regulation by SAMHD1.

Targeting DCs has been deemed an attractive strategy to improve the effectiveness of current vaccine technologies. In the past decade, more than 100 preclinical studies have analysed DC-targeting approaches and their effectiveness in inducing T-cell and antibody responses[45]. However, it remains unclear whether DC-targeting vaccines will be superior to non-specific vaccines. We have shown that the DVLP-encapsulated mRNA induced greater production of spike-specific IgG than its non-specific VLP and LNP counterparts in mice by approximately one order of magnitude. Importantly, DVLPs more efficiently elicited a T-cell response than their non-specific VLP and LNP counterparts, which may be an essential property of therapeutic vaccines developed to remove an established virus infection or to cure cancer.

The future applications of DVLP-based mRNA vaccines include an in situ DC vaccine to cure cancer or to remove established viral infections, such as hepatitis B virus and human papilloma virus infections, possibly in combination with immune checkpoint inhibitors. Furthermore, the potency of DVLP–mRNA vaccines may be further improved by using circular RNA or self-amplifying RNA, which may extend antigen expression and lower the necessary dose for vaccination, thereby improving their efficacy while reducing their cost.

Methods

Cell culture

293T, HeLa, Huh-7, DC2.4, Vero, and Vero E6 cells and human PBMCs were cultured in Dulbecco's modified Eagle's medium (DMEM; Gibco) supplemented with 10% foetal bovine serum (FBS, Gibco) and 1% penicillin/streptomycin (P/S; Thermo Fisher Scientific). Primary splenocytes, mouse glial cells and THP-1 cells were cultured in Roswell Park Memorial Institute (RPMI) 1640 medium (Gibco) with 10% FBS. THP-1 cells were differentiated into macrophage-like cells by treatment with 150 nM phorbol 12-myristate 13-acetate (Sigma-Aldrich, P8139) before the experiment. mBMDCs were generated by culturing freshly isolated bone marrow cells from C57BL/6J mice in RPMI 1640 medium supplemented with 20 ng ml^{-1} granulocyte–macrophage colony-stimulating factor (PeproTech, 315-03), 10% FBS, and 1% P/S for 7 days. Human T cells were isolated from PBMCs using human $CD3^+$ magnetic beads (Miltenyi Biotec, 130-097-043) according to the manufacturer's protocol and were stimulated with 50 IU ml^{-1} IL-2 (Miltenyi Biotec, 130-097-743) and human T Cell TransAct (Miltenyi Biotec, 130-128-758). Murine hepatocytes were isolated from C57BL/6J mice using type I collagenase (Sigma-Aldrich, 10269638001) and cultured in DMEM supplemented with 10% FBS (Gibco) and 1% P/S.

Plasmids

pCCL-PGK-spike-flag(pCCL-PGK is a lentiviral transfer vector construct containing phosphoglycerate kinase (PGK) promoter for transferred gene expression) and pCCL-PGK-spike-mut-flag were constructed by replacing the *GFP* gene in pCCL-PGK-eGFP with the spike or mutant spike (K1003P and V1004P) gene. pCMV-spike-mut-6×MS2 (plasmid containing the cytomegalovirus (CMV) promoter for mRNA expression), pCMV-spike-6×MS2-flag, pCMV-spike-mut-6×MS2-flag and pCMV-gB1-gD1-6×MS2 were generated by inserting six MS2 stem–loop repeats between the stop codon of the spike (or mutant spike or *gB1–gD1* genes) and the polyA sequence, while the whole expression cassette was under the control of a cytomegalovirus promoter.

Production of VLP, IDLV and pseudovirus

VLPs, IDLVs and pseudoviruses were produced by 293T cells in 15 cm dishes. The cells were seeded in the 15 cm dish at a density of 1.35×10^7 per dish 24 h before calcium phosphate transfection. The media were refreshed 12 h after transfection, and at 48 h and 72 h post transfection, the supernatants were filtered through a 0.45 μm filter (Millipore) and ultracentrifuged at 4 °C for 2 h. The resulting pellets were re-suspended in PBS and stored at −80 °C. To produce GFP-expressing spike pseudoviruses and IDLVs (IDLV-spike or IDLV-spike-mut), the cells were transfected with 9.07 μg pMD.2G (or corresponding spike plasmids), 7.26 μg pRSV-Rev (encoding HIV-1 Rev protein), 31.46 μg pMDlg/pRRE-D64V (encoding integrase deficient lentiviral GagPol) or 31.46 μg pCCL-PGK-eGFP (or pCCL-PGK-spike-flag or pCCL-PGK-spike-mut-flag). To produce VSV-G VLP–spike and VSV-G VLP–spike-mut (or SV-G VLP), the cells were transfected with 9.07 μg pMD.2G (or pCMV-SV-G-mut), 7.26 μg pRSV-Rev, 15.73 μg pMDlg/pRRE-D64V, 15.73 μg pMS2M-PH-gagpol-D64V, 31.46 μg pCMV-spike-6×MS2 or pCMV-spike-mut-6×MS2, or their flag and GFP versions. To produce luciferase-encoding spike (or B1.617.2 spike) pseudoviruses, 293T cells were transfected with 20 μg pcDNA3.1-SARS-Cov2-spike (or pcDNA3.1-SARS-Cov2-B1.617.2 spike) and 20 μg pNL4-3.luc.RE.

Transmission electron microscope imaging

Ten microlitres of VLP solution was pipetted onto copper transmission electron microscope grids (200 mesh), and negative staining was performed. Ten microlitres of 2% uranyl acetate (10 μl) was pipetted onto the samples, and they were incubated for 10 min. The solution was removed, and excess buffer was dried with filter paper. Images were digitally recorded using a ×150,000–250,000 magnification CCD Gatan 832 camera (Tecnai G2 Spirit Biotwin; FEI).

Western blotting

To detect the spike protein associated with VLPs or IDLVs, western blotting was performed with or without PNGase F (New England Biolabs, P0704L) treatment. One hundred nanograms of p24 particles was incubated with Glycoprotein Denaturing Buffer at 98 °C for 10 min. After adding GlycoBuffer 2 and NP-40 (10%), the mixtures were incubated with or without 100 units of PNGase F at 37 °C for 2 h. The resulting mixtures were then incubated with sodium dodecyl sulphate (SDS) loading buffer (Beyotime Biotechnology, P0015L) before sample loading. To detect spike protein expressed in cells, 293T cells were lysed in radioimmunoprecipitation assay buffer 36 h after being transduced with VLPs or IDLV. The lysates were incubated with SDS loading buffer supplemented with 2.5% β-mercaptoethanol (Macklin, M828395) at 37 °C for 30 min without boiling. The proteins were separated by SDS–polyacrylamide gel electrophoresis and transferred to polyvinylidene fluoride membranes. The membranes were blocked with 5% fat-free milk dissolved in Tris-buffered saline plus 0.05% Tween-20 for 1 h. To detect the spike protein associated with VLPs or IDLVs, the membranes were cut guided by a molecular weight marker and incubated with an anti-flag monoclonal antibody (mAb; 1:5,000, Sigma-Aldrich, F2555) or an anti-HIV-1 p24 mAb (1:1,000; Santa Cruz Biotechnology, sc69728) overnight at 4 °C, followed by incubation with an anti-rabbit secondary antibody (1:10,000; Cell Signaling Technology, 7074) or an anti-mouse secondary antibody (1:10,000, Cell Signaling Technology, 7076). To detect the spike protein expressed in cells, the membranes were cut guided by a molecular weight marker and incubated with an anti-flag mAb (1:1,000, Sigma-Aldrich, F3165) or an anti-β-actin mAb (1:5,000, Proteintech, 60008) overnight at 4 °C. The membranes were then incubated with anti-mouse secondary antibodies (1:2,500, Cell Signaling Technology, 7076) for 1 h at room temperature.

To detect the spike protein translated from the mRNA in the VLPs, VSV-G VLP–S-mut (full length) and VSV-G VLP–S-mut-ΔTM-CT (without transmembrane domain and cytoplasmic tail) were directly used as virus samples or transduced into 293T cells for protein expression. The cells were collected and lysed in cell lysis buffer (Beyotime Biotechnology, P0013) 24 h after transduction. Anti-spike (1:2,000, Genetex, GTX632604), t-p24 (1:10,000, Abcam, ab63958) and anti-GAPDH (1:10,000, Proteintech, 60004-1-Ig) mAbs were used to detect the indicated proteins. Proteins were visualized using an Amersham Imager 600 instrument (GE Healthcare).

Quantitative PCR

To determine the number of spike mRNAs carried by the VLPs, total RNA was extracted from all samples using a viral DNA/RNA extraction kit (TaKaRa, 9766), followed by complementary DNA synthesis using HiScript III RT SuperMix for qPCR (Vazyme, R323-01) according to the manufacturer's protocol. RT-qPCR was performed using ChamQ Universal SYBR qPCR Master Mix (Vazyme, Q711) following the manufacturer's protocol. The plasmid pLV-PGK-S-mut, diluted to 10^3, 10^4, 10^5, 10^6 and 10^7 copies per μl, was used to construct a standard curve for quantification. To detect the copy number of spike mRNA in each SV-G VLP (GFP), 150 ng p24 SV-G VLP (GFP) and lenti-GFP was used to extract total RNA. RT-qPCR data were normalized to the lenti-GFP copy number.

To analyse viral RNA in tissues, total RNA was extracted from lung samples using RNA Isolator (Vazyme, R401-01) according to the manufacturer's protocol. The SARS-Cov-2 viral load was determined following reverse transcription. To quantify the HSV-1 genome copies in mouse skin or neural tissue, genomic DNA and viral DNA were extracted and subjected to qPCR analysis using ChamQ Universal SYBR qPCR Master Mix (Vazyme, Q711).

To analyse the biodistribution of spike mRNA in vivo, C57BL/6J mice were vaccinated via footpad injection with PBS (50 μl), LNP–spike mRNA (10 μg), VSV-G VLP–spike mRNA (2 μg p24) or SV-G VLP–spike

mRNA (2 μg p24). The mice were euthanized 12 h after vaccination. Various organs and tissues were collected to extract RNA for RT-qPCR analysis, as previously described.

To analyse the innate immune response, cells were transfected with 2 μg poly(I:C), IVT unmodified mRNA (2 μg), or IVT modified mRNA (2 μg), or transduced with VSV-G VLP (500 ng p24). RNA was collected at the indicated time points for the detection of Rig-i, Ifnb1 and Isg15.

To analyse the potential reverse transcription of spike mRNA carried by VLPs, 293T cells were seeded onto 12-well plates at a density of 2×10^5 cells per well and transduced with VSV-G VLP (500 ng p24). pCMV-Spike-mut-6×MS2 (2 μg) transfection was used as a control. Five days later, DNA was extracted for quantification by qPCR. The primers used in these experiments are listed in Supplementary Table 1.

Mice

Six- to eight-week-old, male, specific-pathogen-free C57BL/6 mice or hACE2-transgenic mice were inoculated with VLPs, IDLVs, PBS or LNPs by footpad injection. The mice were killed by cervical dislocation under isoflurane. The animal study complied with the guidelines of the Institutional Animal Care and Use Committee of Shanghai Jiao Tong University and the Wuhan Institute of Virology, Chinese Academy of Sciences.

ELISA

An HIV p24 ELISA (Biodragon Immunotechnologies, BF06203) was used to measure the p24 concentration in the lentiviral particles according to the manufacturer's instructions. To detect SARS-CoV-2-spike-specific antibodies in vivo, sera from the mice were used to detect spike-specific IgG using a mouse IgG ELISA (Bethyl, E99-131) with some modifications. A 200 ng mixture of spike subunits (S1, Novoprotein, DRA35; S2, Novoprotein, DRA48), recombinant full-length spike (Novoprotein, DRA49) or p24 proteins (Novoprotein, DRA19) was used to coat 96-well ELISA plates overnight at 4 °C in a carbonating buffer (pH 9.5). The plates were blocked with PBS containing 0.05% Tween 20 and 1% bovine serum albumin (BSA) for 1 h. Anti-spike (GeneTex, GTX632604) or anti-p24 (Santa Cruz Biotechnology, sc-69728) mAbs were diluted in a fourfold gradient from 20 ng μl^{-1} as the standard curve. After five washes with ELISA wash buffer, horseradish peroxidase-conjugated anti-mouse IgG was diluted in 1% BSA and incubated at room temperature for 1 h. The substrate 3,3′,5,5′-tetramethylbenzidine (Solarbion, PR1210) was added to the plate at 100 μl per well and left for 15 min in the dark. After five washes, the reaction was quenched by the addition of 100 μl per well of ELISA stop solution (Solarbion, C1058), and the absorbance was measured at 450 nm. For serum chemistry assays, ALT and BUN concentrations were determined using mouse ELISA kits (ALT, Coibo, CB10203-Mu; BUN, Coibo, CB10533-Mu).

ELISpot assays

To determine the involvement of cellular immunity, cytokine production by splenic cells in vitro was measured upon treatment with spike peptides. Spleens were removed aseptically, placed in RPMI 1640 medium, gently homogenized, and passed through a cell strainer (Jet Bio-Filtration) to generate single-cell suspensions. Erythrocytes were rapidly washed and lysed with RBC Lysis Buffer (Sangon Biotech, B541001), and the splenocytes were resuspended in 1 ml RPMI 1640 medium. The splenocytes were then seeded at 5×10^5 cells per well in ELISpot plates precoated with anti-mouse IFN-γ, IL-2 or TNF-α antibodies (Mabtech, 3321-4HST-2, 3441-4APW-2 and 3511-4APW-2, respectively). The cells were incubated with a pool of SARS-CoV-2 spike peptides (GenScript, RP30230) at 0.2 μg per well per peptide for 36 h, with 2 μg ml^{-1} concanavalin A (Sigma-Aldrich, C2010) and culture medium as the controls. The detection procedure was performed according to the manufacturer's instructions. Spots were counted and analysed using a Mabtech IRIS FluoroSpot/ELISpot reader.

Neutralization assays

To determine the serum neutralization activity against the GFP-expressing spike pseudovirus, sera from vaccinated mice (40× dilution) were incubated with a GFP-expressing spike pseudovirus at 37 °C for 1 h before adding to Huh-7 cells (4×10^4 cells per well in 48-well plates). The media were changed after 12 h, and photos were taken at 48 h post infection. To perform neutralization assays for the luciferase-encoding spike pseudovirus and SARS-CoV-2 delta strain pseudovirus, serial dilutions of mice sera were incubated with pseudovirus at 37 °C for 1 h before adding to Huh-7 cells (10^4 cells per well in 96-well plates). The culture media were refreshed 12 h post infection, followed by an additional 48 h incubation. Huh-7 cells were subsequently lysed with 50 μl lysis reagent, and 30 μl of the resulting lysates was transferred to 96-well Costar flat-bottom luminometer plates (Corning Costar) for the detection of relative light units using the Firefly Luciferase Assay Kit (Promega, E1500) with an Ultra 384 luminometer (Tecan). Nonlinear regression analysis was performed on the resulting curves using Prism 8 (GraphPad) to calculate EC_{50} values. Neutralization assays with live SARS-CoV-2 (nCoV-2019 BetaCoV/Wuhan/WIV04/2019) were performed in a biosafety level-3 facility with strict adherence to institutional regulations. Sera were heat inactivated and tested at a starting dilution of 1:40 and were serially diluted fourfold to a final dilution of 1:40,960. After incubation of the serum samples with 80 p.f.u. of SARS-CoV-2 for 1 h at 37 °C, the virus–serum mixtures were added to Vero E6 cell monolayers. Supernatants were replaced with 1% low-melting-point agar (Sangon Biotech, A600015) in DMEM with 2% FBS and 1% P/S at 1 h post infection. After 3 days of culture, the plates were fixed and stained to determine the number of plaques. The neutralization titre of each sample was defined as the serum dilution at which the plaques were reduced by 50% (EC_{50}) compared with the virus-positive control wells (virus$^+$ cells). The EC_{50} calculation was based on the nonlinear fitting of the inhibition rate of the positive control wells using GraphPad Prism 8. The HSV-1 and HSV-2 neutralizing antibody titres were tested at a starting dilution of 1:10 and were serially diluted twofold to a final dilution of 1:1,280. After incubation of the serum samples with 50 p.f.u. of HSV-1 or HSV-2 for 1 h at 37 °C, the mixtures were added to Vero cells for 1 h and replaced with 1% low-melting-point agar in DMEM.

RNA immunoprecipitation

For RIP, 293T cells were transfected with pCCL-PGK-spike, pCMV-spike-mut-6×MS2 or pMS2M-PH-gagpol-D64V (encoding fusion protein of bacteriophage MS2 coat protein and lentiviral GagPol polyprotein) alone or in combination, depending on the aim of the experiment. After 48 h, the cells were washed three times with PBS and centrifuged at 1,000 × *g* for 5 min. The resulting pellets were resuspended in RIP lysis buffer (10 mM HEPES (Beyotime, ST2425), 200 mM NaCl (SCR, 10019318), 20 mM EDTA-Na_2 (Beyotime, ST1308), 0.5% Triton (Beyotime, ST795), RNase inhibitor (Beyotime, R0102), phenylmethylsulphonyl fluoride (Beyotime, ST506) and dithiothreitol (Beyotime, ST041)) and incubated at 4 °C for 1 h. After centrifugation at 12,000 × *g* for 10 min, the supernatants were incubated with an anti-MS2 coat protein antibody (Merck, ABE76-I) at 4°C for 4 h; then, protein A/G (Santa Cruz Biotechnology, sc-2003) was added, followed by incubation at 4 °C for 4 h. The beads were washed three times with RIP lysis buffer and then subjected to RNA isolation and reverse transcription to generate cDNA. The cDNA samples were analysed by qPCR using the spike-specific primer sequences, as listed in Supplementary Table 1.

Flow cytometry analysis

For DC2.4 and HeLa cells, 4×10^4 cells were infected with 100 ng p24 VLPs (GFP version). The cells were collected 3 days after infection. GFP$^+$ cells were analysed by flow cytometry (BD FACSDiva 7; BD Biosciences). mBMDCs were generated from the bone marrow cells of C57BL/6J mice and cultured in RPMI 1640 medium supplemented with serum containing 20 ng ml^{-1} granulocyte–macrophage colony-stimulating factor

(PeproTech, 315-03-20), 10% FBS and 1% P/S for 7 days. mBMDCs were seeded at a density of 5×10^5 cells per well and transduced with VLPs (GFP version) the next day. GFP and CD11c (Elabscience Biotechnology, E-AB-F0991UH) signals were determined by flow cytometry 3 days after infection. The gating strategies are shown in Supplementary Fig. 18.

Immunofluorescence assays

For immunofluorescence assay, 293T cells were seeded into 48-well plates containing 0.1 mg ml^{-1} poly-D-lysine-coated cover glasses at a density of 4×10^4 cells per well. The following day, the cells were transduced with 150 ng p24 IDLVs or VLPs or transfected with 0.6 μg pCMV-spike-6×MS2 or pCMV-spike-mut-6×MS2 plasmids. The cells were fixed in 4% paraformaldehyde (PFA) 36 h after transduction or transfection. They were then stained with an anti-flag tag antibody (Proteintech, 66008-3-Ig), followed by incubation with Alexa Fluor 555–conjugated IgG (Cell Signaling Technology, 4409) and nuclei staining with 4′,6-diamidino-2-phenylindole (Beyotime Biotechnology, P0131). To evaluate the SARS-CoV-2 distribution in lung tissues, the lungs of mice were fixed in 4% PFA overnight at 4 °C before transferring to 30% sucrose and embedding in optimal cutting temperature compound. Sections were stained with an anti-SARS-CoV-2 NP antibody, and imaging was performed using a confocal microscope (A1Si, Nikon) to verify the expression of spike proteins.

C57BL/6J mice were injected in their footpads with PBS (50 μl), LNP–spike mRNA (10 μg), VSV-G VLP–spike mRNA (2 μg p24) or SV-G VLP–spike mRNA (2 μg p24). They were euthanized 12 h later, and lymph nodes and footpads were collected and evaluated using immunofluorescence assays. Briefly, tissue sections were stained with anti-CD11c (Servicebio, GB11059) and anti-spike antibodies (Genetex, GTX632604), followed by immunostaining with Alexa Fluor 488–conjugated Affinipure donkey anti-rabbit secondary antibodies (Jackson ImmunoResearch Laboratories, 711-547-003) and Alexa Fluor 555–conjugated Affinipure goat anti-mouse secondary antibodies (Huabio, HA1118). 4′,6-Diamidino-2-phenylindole (Beyotime, P0131) was used to stain the nuclei.

In vitro spike mRNA synthesis

The mutant spike mRNA for the LNP–mRNA vaccine was produced by T7 RNA polymerase–mediated IVT (Vazyme, TR101), which incorporated modified (1-methyl-3′-pseudouridine) and unmodified uridine-5′-triphosphate into the S-mut mRNA in a certain ratio. A modified 5′-cap structure (m7G5′ppp5′G) was added using an mRNA Cap 2′-O-Methyltransferase kit (Vazyme, DDf110). The DNA template for in vitro transcription was produced by linearization of a plasmid encoding the full-length mutant spike protein as the S-mut used for the VLPs. The transcription product was purified by phenol/chloroform extraction.

Laboratory LNP generation and encapsulation of mRNA

An mRNA encoding the SARS-CoV-2 spike protein was encapsulated in LNPs as described previously[42,43]. Briefly, dilinoleylmethyl -4-dimethylaminobutyrate, distearoylphosphatidylcholine, cholesterol and polyethylene glycol 2000–dimyristoyl glycerol were dissolved in ethanol at molar ratios of 50:10:38.5:1.5. The lipids were dissolved in ethanol, and the mRNA was dissolved in citrate buffer (50 mM, pH 3.0). The two formulations were rapidly mixed at a ratio of 3:1 by volume and incubated for 10 min. The LNP–mRNA formulation was dialysed against PBS in dialysis cassettes for 16 h.

Laboratory LNP vaccination in mice

To compare DLVP–S-mut with laboratory LNPs, 6- to 8-week-old male C57BL/6 mice were inoculated with DLVP–S-mut (2 μg p24) or the LNP–mRNA vaccine (2 μg or 10 μg) via footpad injection. Sera were collected from the mice 12 days after incubation to detect SARS-CoV-2-specific IgG by ELISA. Cytokine production by splenocytes was measured using ELISpot assays.

SARS-CoV-2 challenge in hACE2 transgenic mice

hACE2-transgenic mice ($n = 6$) at 6 to 8 weeks of age were inoculated with 1.5 μg p24 VLP–mRNA and administered a booster injection at day 14 (1.5 μg p24), with footpad PBS injection used as a control. The mice were challenged with a 10^5 50% tissue culture infectious dose of SARS-CoV-2 via intranasal administration on day 28 post immunization. Three days after the live virus challenge, all mice were killed for histopathological and virological analyses.

Histopathology

Tissues were fixed in 4% formaldehyde and embedded in paraffin. Lung and skin sections were stained with H&E. For immunohistochemistry, the sections were treated with 3% hydrogen peroxide for 25 min to block endogenous peroxidase activity. The sections were then blocked with 3% BSA at room temperature for 30 min and incubated with anti-CD4 (1:100; Servicebio, gb13064) or anti-CD8 (1:1,000; Servicebio, gb11068) antibodies at 4 °C overnight. The sections were then incubated with an anti-rabbit secondary antibody (1:500; Servicebio, gb23303), followed by incubation with a freshly prepared 3,3′-diaminobenzidinesubstrate solution to detect bound antibody. The sections were counterstained with haematoxylin and then with aqueous ammonia, dehydrated and cover-slipped.

Plaque assays

To quantify infectious SARS-CoV-2 particles in the lung, endpoint titrations were performed on confluent Vero E6 cells. Lung homogenates were serially diluted in DMEM supplemented with 2% FBS and 1% P/S and incubated with cells for 2 h at 37 °C. The supernatants were then replaced with 1% low-melting-point agar in DMEM with 2% FBS and 1% P/S. The plates were inverted and incubated at 37 °C for 3 days. They were then fixed with 4% PFA for 10 min at room temperature and stained with 1 ml 1% crystal violet for 1.5 h. The plaques were counted manually. HSV-1 and HSV-2 titres were determined in a similar manner using confluent Vero cells. The viral load was calculated based on the plaque count and the dilution factor.

HSV-1 challenge in mice

Six- to eight-week-old C57BL/J6 mice ($n = 4$) were inoculated with VLP–*gB1–gD1* mRNA (1.5 μg p24) or PBS by footpad injection and administered a booster injection on day 14 (1.5 μg p24). Fourteen days after the booster immunization, the mice were depilated on the dorsal surface near the spine, and 16 gentle scrapes were made on the skin surface with disposable sandpaper before challenge of the abraded skin with 10^7 p.f.u. of HSV-1 17syn$^+$ in a 10 μl solution. Serum samples were collected for neutralization assays. Skin graphs were collected at the indicated times after infection. Six days after HSV-1 infection, the mouse skin samples were processed for H&E staining, plaque assays or DNA isolation.

Statistical analyses

Data are presented as the mean ± standard error of the mean (s.e.m.) for all experiments. One-way analysis of variance (ANOVA), unpaired two-tailed Student's *t*-tests or paired two-tailed Wilcoxon tests were performed to determine the *P* values. The level of statistical significance is indicated by asterisks (*$P < 0.05$; **$P < 0.01$; ***$P < 0.001$; NS, non-significant).

Reporting summary

Further information on research design is available in the Nature Portfolio Reporting Summary linked to this article.

Data availability

Source data for the figures are available from figshare[51] at https://doi.org/10.6084/m9.figshare.24516694. The raw and analysed datasets generated during the study are available for research purposes from

the corresponding authors on reasonable request. Source data are provided with this paper.

References

1. Roth, G. A. et al. Designing spatial and temporal control of vaccine responses. *Nat. Rev. Mater.* **7**, 174–195 (2022).
2. Colby, D. J. et al. Safety and immunogenicity of Ad26 and MVA vaccines in acutely treated HIV and effect on viral rebound after antiretroviral therapy interruption. *Nat. Med.* **26**, 498–501 (2020).
3. Ng'uni, T., Chasara, C. & Ndhlovu, Z. M. Major scientific hurdles in HIV vaccine development: historical perspective and future directions. *Front. Immunol.* **11**, 590780 (2020).
4. Bernstein, D. I. et al. The R2 non-neuroinvasive HSV-1 vaccine affords protection from genital HSV-2 infections in a guinea pig model. *npj Vaccines* **5**, 104 (2020).
5. Awasthi, S. et al. Nucleoside-modified mRNA encoding HSV-2 glycoproteins C, D, and E prevents clinical and subclinical genital herpes. *Sci. Immunol.* **4**, eaaw7083 (2019).
6. Wang, W. et al. Dual-targeting nanoparticle vaccine elicits a therapeutic antibody response against chronic hepatitis B. *Nat. Nanotechnol.* **15**, 406–416 (2020).
7. Roden, R. B. S. & Stern, P. L. Opportunities and challenges for human papillomavirus vaccination in cancer. *Nat. Rev. Cancer* **18**, 240–254 (2018).
8. Sahin, U. et al. Personalized RNA mutanome vaccines mobilize poly-specific therapeutic immunity against cancer. *Nature* **547**, 222–226 (2017).
9. Keskin, D. B. et al. Neoantigen vaccine generates intratumoral T cell responses in phase Ib glioblastoma trial. *Nature* **565**, 234–239 (2019).
10. Polack, F. P. et al. Safety and efficacy of the BNT162b2 mRNA COVID-19 vaccine. *N. Engl. J. Med.* **383**, 2603–2615 (2020).
11. Baden, L. R. et al. Efficacy and safety of the mRNA-1273 SARS-CoV-2 vaccine. *N. Engl. J. Med.* **384**, 403–416 (2021).
12. Widge, A. T. et al. Durability of responses after SARS-CoV-2 mRNA-1273 vaccination. *N. Engl. J. Med.* **384**, 80–82 (2021).
13. Thomas, S. J. et al. Safety and efficacy of the BNT162b2 mRNA COVID-19 vaccine through 6 months. *N. Engl. J. Med.* **385**, 1761–1773 (2021).
14. Wang, Y. et al. mRNA vaccine: a potential therapeutic strategy. *Mol. Cancer* **20**, 33 (2021).
15. Lindsay, K. E. et al. Visualization of early events in mRNA vaccine delivery in non-human primates via PET–CT and near-infrared imaging. *Nat. Biomed. Eng.* **3**, 371–380 (2019).
16. Chen, J. et al. Lipid nanoparticle-mediated lymph node-targeting delivery of mRNA cancer vaccine elicits robust $CD8^+$ T cell response. *Proc. Natl Acad. Sci. USA* **119**, e2207841119 (2022).
17. Tenforde, M. W. et al. Effectiveness of severe acute respiratory syndrome coronavirus 2 messenger RNA vaccines for preventing coronavirus disease 2019 hospitalizations in the United States. *Clin. Infect. Dis.* **74**, 1515–1524 (2022).
18. Eisenbarth, S. C. Dendritic cell subsets in T cell programming: location dictates function. *Nat. Rev. Immunol.* **19**, 89–103 (2019).
19. Lanzavecchia, A. & Sallusto, F. Regulation of T cell immunity by dendritic cells. *Cell* **106**, 263–266 (2001).
20. Heath, W. R., Kato, Y., Steiner, T. M. & Caminschi, I. Antigen presentation by dendritic cells for B cell activation. *Curr. Opin. Immunol.* **58**, 44–52 (2019).
21. Wykes, M., Pombo, A., Jenkins, C. & MacPherson, G. G. Dendritic cells interact directly with naive B lymphocytes to transfer antigen and initiate class switching in a primary T-dependent response. *J. Immunol.* **161**, 1313–1319 (1998).
22. Igyarto, B. Z., Jacobsen, S. & Ndeupen, S. Future considerations for the mRNA-lipid nanoparticle vaccine platform. *Curr. Opin. Virol.* **48**, 65–72 (2021).
23. Blumenthal, K. G. et al. Delayed large local reactions to mRNA-1273 vaccine against SARS-CoV-2. *N. Engl. J. Med.* **384**, 1273–1277 (2021).
24. Yu, Y. et al. Antibody-dependent cellular cytotoxicity response to SARS-CoV-2 in COVID-19 patients. *Signal Transduct. Target. Ther.* **6**, 346 (2021).
25. Svajger, U., Anderluh, M., Jeras, M. & Obermajer, N. C-type lectin DC-SIGN: an adhesion, signalling and antigen-uptake molecule that guides dendritic cells in immunity. *Cell. Signal.* **22**, 1397–1405 (2010).
26. Yang, L. et al. Engineered lentivector targeting of dendritic cells for in vivo immunization. *Nat. Biotechnol.* **26**, 326–334 (2008).
27. Wrapp, D. et al. Cryo-EM structure of the 2019-nCoV spike in the prefusion conformation. *Science* **367**, eabb2507 (2020).
28. Yin, D. et al. Targeting herpes simplex virus with CRISPR-Cas9 cures herpetic stromal keratitis in mice. *Nat. Biotechnol.* **39**, 567–577 (2021).
29. Ling, S. et al. Lentiviral delivery of co-packaged Cas9 mRNA and a Vegfa-targeting guide RNA prevents wet age-related macular degeneration in mice. *Nat. Biomed. Eng.* **5**, 144–156 (2021).
30. Segel, M. et al. Mammalian retrovirus-like protein PEG10 packages its own mRNA and can be pseudotyped for mRNA delivery. *Science* **373**, 882–889 (2021).
31. Banskota, S. et al. Engineered virus-like particles for efficient in vivo delivery of therapeutic proteins. *Cell* **185**, 250–265.e16 (2022).
32. Hu, B., Tai, A. & Wang, P. Immunization delivered by lentiviral vectors for cancer and infectious diseases. *Immunol. Rev.* **239**, 45–61 (2011).
33. Chang, D. & Zaia, J. Why glycosylation matters in building a better flu vaccine. *Mol. Cell. Proteomics* **18**, 2348–2358 (2019).
34. Watanabe, Y., Allen, J. D., Wrapp, D., McLellan, J. S. & Crispin, M. Site-specific glycan analysis of the SARS-CoV-2 spike. *Science* **369**, eabb9983 (2020).
35. Neerukonda, S. N. et al. Establishment of a well-characterized SARS-CoV-2 lentiviral pseudovirus neutralization assay using 293T cells with stable expression of ACE2 and TMPRSS2. *PLoS ONE* **16**, e0248348 (2021).
36. Wienert, B., Shin, J., Zelin, E., Pestal, K. & Corn, J. E. In vitro-transcribed guide RNAs trigger an innate immune response via the RIG-I pathway. *PLoS Biol.* **16**, e2005840 (2018).
37. Mu, X., Greenwald, E., Ahmad, S. & Hur, S. An origin of the immunogenicity of in vitro transcribed RNA. *Nucleic Acids Res.* **46**, 5239–5249 (2018).
38. Ying, T. et al. Exceptionally potent neutralization of Middle East respiratory syndrome coronavirus by human monoclonal antibodies. *J. Virol.* **88**, 7796–7805 (2014).
39. Ma, M. L. et al. Systematic profiling of SARS-CoV-2-specific IgG responses elicited by an inactivated virus vaccine identifies peptides and proteins for predicting vaccination efficacy. *Cell Discov.* **7**, 67 (2021).
40. Jiang, H. W. et al. SARS-CoV-2 proteome microarray for global profiling of COVID-19 specific IgG and IgM responses. *Nat. Commun.* **11**, 3581 (2020).
41. Li, Y. et al. Linear epitope landscape of the SARS-CoV-2 Spike protein constructed from 1,051 COVID-19 patients. *Cell Rep.* **34**, 108915 (2021).
42. Lu, J. et al. A COVID-19 mRNA vaccine encoding SARS-CoV-2 virus-like particles induces a strong antiviral-like immune response in mice. *Cell Res.* **30**, 936–939 (2020).
43. Cheng, Q. et al. Selective organ targeting (SORT) nanoparticles for tissue-specific mRNA delivery and CRISPR-Cas gene editing. *Nat. Nanotechnol.* **15**, 313–320 (2020).
44. Bao, L. et al. The pathogenicity of SARS-CoV-2 in hACE2 transgenic mice. *Nature* **583**, 830–833 (2020).

45. Kastenmuller, W., Kastenmuller, K., Kurts, C. & Seder, R. A. Dendritic cell-targeted vaccines—hope or hype? *Nat. Rev. Immunol.* **14**, 705–711 (2014).
46. Ku, M.-W., Charneau, P. & Majlessi, L. Use of lentiviral vectors in vaccination. *Expert Rev. Vaccines* **20**, 1571–1586 (2021).
47. Pollack, S. M. et al. First-in-human treatment with a dendritic cell-targeting lentiviral vector-expressing NY-ESO-1, LV305, induces deep, durable response in refractory metastatic synovial sarcoma patient. *J. Immunother.* **40**, 302–306 (2017).
48. Ku, M. W. et al. Lentiviral vector induces high-quality memory T cells via dendritic cells transduction. *Commun. Biol.* **4**, 713 (2021).
49. Ku, M. W. et al. Intranasal vaccination with a lentiviral vector protects against SARS-CoV-2 in preclinical animal models. *Cell Host Microbe* **29**, 236–249.e6 (2021).
50. Norton, T. D. & Miller, E. A. Recent advances in lentiviral vaccines for HIV-1 infection. *Front. Immunol.* **7**, 243 (2016).
51. Zhong, Y. SD_FIG1-7.xlsx.xlsx. *figshare* https://doi.org/10.6084/m9.figshare.24516694 (2023).

Acknowledgements

Y.C. is supported by the National Key R&D Program of China (2022YFC3400205), the National Natural Science Foundation of China (31971364) and Shanghai Jiao Tong University Scientific and Technological Innovation Funds (AF4150049). J.H. is supported by the National Natural Science Foundation of China (81970766 and 82171102) and the Shanghai Innovation Development Program (2020-RGZN-02033). T.Y. is supported by the National Key R&D Program of China (2019YFA0904400) and the National Natural Science Foundation of China (81822027 and 81630090). S.T. is supported by the National Natural Science Foundation of China (31970130) and the National Key R&D Program of China (2020YFE0202200).

Author contributions

Y.C. conceived the study and designed the experiments; D.Y., Y. Zhong, S. Ling, S. Lu, Xiaoyuan Wang, Z.J., J.W., Y.D., X.T., Q.H., Xingbo Wang, J.C., Z.L., Y.L., Z.X., H.J., Y.W., Y.S., Q.W., J.X., W.H., H.X., H.Y., Y. Zhang, L.D., Z.H., S.T., R.D., T.Y. and J.H. performed the experiments or provided essential experimental resources; all the authors analysed the data; Y. Zhong, D.Y., S. Ling, and Y.C. wrote the manuscript with help from all the authors.

Competing interests

Y.C. is a co-founder and advisor of BDGENE Therapeutics. The other authors declare no competing interests.

Additional information

Supplementary information The online version contains supplementary material available at https://doi.org/10.1038/s41551-024-01208-4.

Correspondence and requests for materials should be addressed to Jiaxu Hong or Yujia Cai.

Peer review information *Nature Biomedical Engineering* thanks Ke Cheng and the other, anonymous, reviewer(s) for their contribution to the peer review of this work. Peer reviewer reports are available.

nature portfolio

Corresponding author(s): Yujia Cai

Last updated by author(s): Nov 6, 2023

Reporting Summary

Nature Portfolio wishes to improve the reproducibility of the work that we publish. This form provides structure for consistency and transparency in reporting. For further information on Nature Portfolio policies, see our Editorial Policies and the Editorial Policy Checklist.

Statistics

For all statistical analyses, confirm that the following items are present in the figure legend, table legend, main text, or Methods section.

n/a	Confirmed	
☐	☒	The exact sample size (*n*) for each experimental group/condition, given as a discrete number and unit of measurement
☐	☒	A statement on whether measurements were taken from distinct samples or whether the same sample was measured repeatedly
☐	☒	The statistical test(s) used AND whether they are one- or two-sided *Only common tests should be described solely by name; describe more complex techniques in the Methods section.*
☒	☐	A description of all covariates tested
☐	☒	A description of any assumptions or corrections, such as tests of normality and adjustment for multiple comparisons
☐	☒	A full description of the statistical parameters including central tendency (e.g. means) or other basic estimates (e.g. regression coefficient) AND variation (e.g. standard deviation) or associated estimates of uncertainty (e.g. confidence intervals)
☐	☒	For null hypothesis testing, the test statistic (e.g. *F*, *t*, *r*) with confidence intervals, effect sizes, degrees of freedom and *P* value noted *Give P values as exact values whenever suitable.*
☒	☐	For Bayesian analysis, information on the choice of priors and Markov chain Monte Carlo settings
☒	☐	For hierarchical and complex designs, identification of the appropriate level for tests and full reporting of outcomes
☒	☐	Estimates of effect sizes (e.g. Cohen's *d*, Pearson's *r*), indicating how they were calculated

Our web collection on statistics for biologists contains articles on many of the points above.

Software and code

Policy information about availability of computer code

Data collection	BD FACSDiva version 7 was used to collect flow-cytometry data. The Roche LightCycler 96 Real-Time PCR system was used to collect real-time PCR data. Western blot data were collected via an Amersham ImageQuant 680 system. Fluorescence image data were collected using a laser scanning confocal microscope (A1si, Nikon). Haematoxylin & Eosin staining and immunohistochemistry images were collected using a fluorescence microscope (Eclipse Ni, Nikon).
Data analysis	GraphPad Prism 8, ImageJ 1.52v, FlowJo 7.6, Case viewer 2.4v.

For manuscripts utilizing custom algorithms or software that are central to the research but not yet described in published literature, software must be made available to editors and reviewers. We strongly encourage code deposition in a community repository (e.g. GitHub). See the Nature Portfolio guidelines for submitting code & software for further information.

Data

Policy information about availability of data

All manuscripts must include a data availability statement. This statement should provide the following information, where applicable:

- Accession codes, unique identifiers, or web links for publicly available datasets
- A description of any restrictions on data availability
- For clinical datasets or third party data, please ensure that the statement adheres to our policy

Source data for the figures are provided with this paper, and also available from figshare at http://doi.org/10.6084/m9.figshare.24516694. The raw and analysed datasets generated during the study are available for research purposes from the corresponding authors on reasonable request.

Research involving human participants, their data, or biological material

Policy information about studies with human participants or human data. See also policy information about sex, gender (identity/presentation), and sexual orientation and race, ethnicity and racism.

Reporting on sex and gender	The study did not involve human research participants.
Reporting on race, ethnicity, or other socially relevant groupings	–
Population characteristics	–
Recruitment	–
Ethics oversight	–

Note that full information on the approval of the study protocol must also be provided in the manuscript.

Field-specific reporting

Please select the one below that is the best fit for your research. If you are not sure, read the appropriate sections before making your selection.

☒ Life sciences ☐ Behavioural & social sciences ☐ Ecological, evolutionary & environmental sciences

For a reference copy of the document with all sections, see nature.com/documents/nr-reporting-summary-flat.pdf

Life sciences study design

All studies must disclose on these points even when the disclosure is negative.

Sample size	For the in vitro experiments, we used triplicate samples for comparisons between one or multiple groups, followed by statistical tests. For the in vivo studies, at least four mice were used for each group. Sample sizes were chosen to meet or exceed the standards of reproducibility of similar published studies.
Data exclusions	No data were excluded from analysis.
Replication	The experimental findings can be reliably reproduced. Some key data generated by one co-author were repeated by other co-authors.
Randomization	Samples were randomly allocated into experimental groups for the in vitro experiments. Animals were randomly grouped for the in vivo experiments.
Blinding	For the in vivo studies, the body weight was measured blindly.

Reporting for specific materials, systems and methods

We require information from authors about some types of materials, experimental systems and methods used in many studies. Here, indicate whether each material, system or method listed is relevant to your study. If you are not sure if a list item applies to your research, read the appropriate section before selecting a response.

Materials & experimental systems

n/a	Involved in the study
☐	☒ Antibodies
☐	☒ Eukaryotic cell lines
☒	☐ Palaeontology and archaeology
☐	☒ Animals and other organisms
☒	☐ Clinical data
☒	☐ Dual use research of concern
☒	☐ Plants

Methods

n/a	Involved in the study
☒	☐ ChIP-seq
☐	☒ Flow cytometry
☒	☐ MRI-based neuroimaging

Antibodies

Antibodies used

Antibodies used for Western blotting:
Anti-flag antibody (Sigma, F2555), 1:5000;
Anti-β-Actin mouse monoclonal antibody (Proteintech, 60008), 1:5000;
Anti-HIV1-p24 mouse monoclonal antibody (Abcam, ab63958), 1:10000;
Anti-SARS-CoV-2 Spike antibody (GeneTex, GTX632604);
Anti-mouse secondary antibody (Cell Signaling Technology, 7076), 1:2500 or 1:10000;
Anti-rabbit secondary antibody (Cell Signaling Technology, 7074), 1:10000;

Antibodies used for immunofluorescence:
Anti-flag tag antibody (Proteintech, 66008-3-Ig);
Anti-SARS-CoV-2 nucleocapsid antibody (Sino Biological, 40143-R040);
Anti-SARS-CoV-2 Spike antibody (GeneTex, GTX632604);
Anti-CD11c antibody (Servicebio, GB11059);
Alexa Fluor 555 IgG (Cell Signaling Technology, 4409);
Alexa Fluor 488 IgG (Jackson ImmunoResearch, 711-545-152);
TRITC-conjugated goat anti-rabbit immunoglobulin (Easybio, BE0115);

Antibodies used for ELISA:
SARS-CoV-2 (COVID-19) Spike antibody (Genetex, GTX632604);
Anti-p24 antibody (Santa Cruz Biotechnology, sc-69728);
HRP goat anti-mouse IgG (BETHYL, E90-131);
HRP rat anti-mouse IgA (Southern Biotech, 1165-05);

Antibodies used for immunohistochemistry:
Anti-CD4+ (Servicebio, cat: gb13064), 1:100;
Anti-CD8+ (Servicebio, cat: gb11068), 1:1000;
Anti-rabbit secondary antibody (Servicebio, cat: gb23303), 1:500.

Antibodies used for FACS:
PE/Cyanine7 Anti-Mouse CD11c Antibody (Elabscience Biotechnology, E-AB-F0991UH).

Validation

Antibodies were validated for each application using manufacturers guidelines. Multiple dilutions were tested to determine the most appropriate dilution.

Eukaryotic cell lines

Policy information about cell lines and Sex and Gender in Research

Cell line source(s)

293T, Vero, DC2.4, THP-1 and HeLa cells were obtained from the laboratory of Soren Riis Paludan. Vero E6 cells were obtained from Sheng-ce Tao's laboratory. Huh-7 cells were obtained from the laboratory of Ze-guang Han.

Authentication

None of the cell lines used were authenticated.

Mycoplasma contamination

All cell lines tested negative for mycoplasma contamination.

Commonly misidentified lines
(See ICLAC register)

No commonly misidentified cell lines were used.

Animals and other research organisms

Policy information about studies involving animals; ARRIVE guidelines recommended for reporting animal research, and Sex and Gender in Research

Laboratory animals

Six–eight-weeks old, male, specific-pathogen-free (SPF) C57BL/6J and hACE2 mice were used. Mice were housed in an environmentally controlled room (23 °C, with 55±5% humidity and 12-h/12-h light–dark cycle).

Wild animals	The study did not involve wild animals.
Reporting on sex	Sex was not considered in the study.
Field-collected samples	The study did not involve samples collected from the field.
Ethics oversight	The animal study complied with the guidelines of the Institutional Animal Care and Use Committee (IACUC) of Shanghai Jiao Tong University and Wuhan Institute of Virology, Chinese Academy of Sciences. For the SARS-CoV-2 challenge study, the experiments were performed in a BSL-3 facility with all experimental methods carried out following the regulations and guidelines set forth by the Animal Experiments Committee of Wuhan Institute of Virology, Chinese Academy of Sciences. All experimental protocols were approved by the Animal Experiments Committee of Wuhan Institute of Virology, Chinese Academy of Sciences (WIVA17202005).

Note that full information on the approval of the study protocol must also be provided in the manuscript.

Flow Cytometry

Plots

Confirm that:

☒ The axis labels state the marker and fluorochrome used (e.g. CD4-FITC).

☒ The axis scales are clearly visible. Include numbers along axes only for bottom left plot of group (a 'group' is an analysis of identical markers).

☒ All plots are contour plots with outliers or pseudocolor plots.

☒ A numerical value for number of cells or percentage (with statistics) is provided.

Methodology

Sample preparation	Cells were fixed by 0.1 % paraformaldehyde at 4 °C overnight before analysis.
Instrument	LSR Fortessa flow cytometer (BD Biosciences)
Software	BD FACSDiva 7 was used to collect the flow-cytometry data. FlowJo 7.6 was used to analyse data.
Cell population abundance	10,000 cells were acquired from each sample.
Gating strategy	Cells were identified by forward and side scatter, followed by doublet exclusion. The boundary between the positive and negative populations were determined by fluorescence intensity.

☒ Tick this box to confirm that a figure exemplifying the gating strategy is provided in the Supplementary Information.